

Investigation of an ANPC Inverter in Electrified Vehicles

Master of Science Thesis

ZHENGHUA ZHANG

Investigation of an ANPC Inverter in Electrified Vehicles

ZHENGHUA ZHANG



CHALMERS
UNIVERSITY OF TECHNOLOGY

Department of Energy and Environment Technology
Division of Electric Power Engineering
CHALMERS UNIVERSITY OF TECHNOLOGY
Gothenburg, Sweden 2016

Investigation of an ANPC Inverter in Electrified Vehicles
ZHENGHUA ZHANG

© ZHENGHUA ZHANG, 2016.

Supervisor: Torbjörn Thiringer, Department of Energy and Environment Technology
Examiner: Torbjörn Thiringer, Department of Energy and Environment Technology

Department of Energy and Environment Technology
Division of Electric Power Engineering
Chalmers University of Technology
SE-412 96 Gothenburg
Telephone +46 31 772 1000

Cover: Topology of the ANPC inverter.

Typeset in L^AT_EX
Printed by [Chalmers University of Technology]
Gothenburg, Sweden 2016

Investigation of an ANPC Inverter in Electrified Vehicles
ZHENGHUA ZHANG
Department of Energy and Environment Technology
Chalmers University of Technology

Abstract

In this thesis, a three-level active neutral point clamped (ANPC) inverter for a permanent magnet synchronous machine (PMSM) drive is developed and its performance is investigated. The performance investigation is mainly based on comparison with a two level inverter including semiconductor devices' selection, total harmonics distortion (THD) analysis, semiconductor devices losses evaluation as well as energy efficiency study with various drive cycles. Moreover, the losses distribution in the ANPC inverter is also analyzed.

In the initial part of the thesis, theories of electric drive system used in this thesis are introduced. Based on the theories, an ANPC inverter model is built. The modulation strategy is chosen and different switching states are discussed in detail. With the chosen modulation strategy, a space vector modulation (SVM) method is developed and studied carefully. A two level inverter with SVM method is implemented for performance comparison with the ANPC inverter. The simulation results show that the ANPC inverter has obvious total harmonics distortion (THD) reductions for both voltage and current.

To evaluate the inverters' performance in electrified vehicles, an electric vehicle system is set up. The required rated power of the inverter in the system is 125kW at a DC voltage of 800V . Accordingly, each semiconductor device in the ANPC inverter need to withstand a reverse voltage of 400V which is half of that in the two-level inverter, thus an IGBT module with a reverse blocking voltage of 650V is selected for the ANPC inverter while it is 1200V for the two-level inverter. Compared with the two level inverter, the ANPC inverter has lower total losses in the entire operation region. The maximum efficiency of the ANPC inverter can reach as much as 99.25% while it is only 98.68% for the two-level inverter. Furthermore, when operating with various drive cycles, the ANPC inverter has an energy efficiency improvement of 2.86% in the EUDC drive cycles and 0.99% in the ECE drive cycles.

Finally, the losses distribution in the ANPC inverter is analyzed since the unbalancing losses distribution is a significant issue for the ANPC inverter. The losses distribution on each device varies when torque and speed are changing but the most stressed device is the same throughout all operating points. Moreover, with various power factors, the losses are always concentrated on the inner switches.

Keywords: Electrified vehicles, ANPC inverter, Two level inverter, Efficiency evaluation.

Acknowledgements

This thesis has been conducted in the Energy and Environment Department of Chalmers University of Technology.

First of all, I would like to express my sincerely gratitude and thankful to my supervisor and examiner, Prof. Torbjörn Thiringer, for his relentless support and guidance. I would also like to thank Prof. Tarik Abdulahovic for helping me with the software installation of PLECS. I am grateful to the faculties and research staffs in Chalmers, they helped me in different ways during my two-years' study.

My study at Chalmers is supported by the Swedish Institute Scholarship. I would like to express my gratitude to their support.

Finally, I would like to sincerely thank my family for their endless support and understanding during the whole period of this thesis.

Zhenghua Zhang, Gothenburg, June 2016

Table of Contents

Abstract	v
Acknowledgements	vii
Abbreviations	1
1 Introduction	1
1.1 Background and Previous Work	1
1.2 Purpose	2
1.3 Thesis Outline	2
2 Electric Drive System	3
2.1 Electric Drive System	3
2.2 Power Electronics Converters	3
2.2.1 Multilevel inverters	4
2.2.2 Modulation strategies	4
2.2.3 Losses of semiconductor devices	6
2.2.3.1 Conduction losses	6
2.2.3.2 Switching losses	7
2.3 PMSM Modeling	8
2.4 Drive Cycles	9
3 Operation Principle of the ANPC Inverter	11
3.1 Modulation Strategy of ANPC Inverter	11
3.2 SVM Method of ANPC Inverter	13
3.2.1 Space vector diagram of ANPC inverter	13
3.2.2 Sector identification	14
3.2.2.1 Large sector identification	14
3.2.2.2 Sub-sector identification	15
3.2.3 Vector turn-on time calculation	16
3.2.4 Vector operation sequence	17
3.3 Simulation Results	19
3.4 Implementation of Two Level Inverter	22
4 Performance Evaluation of the ANPC Inverter	25
4.1 Case Setup	25
4.1.1 Voltage and current requirement of the electric machine	25

Table of Contents

4.2	Performance Comparison between the Two-level and the ANPC Inverter . .	27
4.2.1	Voltage and Current Comparison	27
4.2.2	Losses and Efficiency Comparison	29
4.2.2.1	Conduction losses	30
4.2.2.2	Switching losses	31
4.2.2.3	Total losses	33
4.2.2.4	Efficiency	34
4.2.3	Efficiency comparison with drive cycles	36
4.2.3.1	ECE drive cycle	36
4.2.3.2	EUDC drive cycle	38
4.3	Losses Distribution of the ANPC Inverter	40
5	Conclusion	43
6	Future Work	45
	References	47

1

Introduction

The development of vehicles has changed people's lifestyles significantly in the past decades. It not only brings great convenience and improvement of travel efficiency, but also large amount of energy consumption and air pollution. The fuel energy crisis and increasing concern for environment issues is driving the vehicles industry toward electrification.

1.1 Background and Previous Work

Electrified vehicles could meet higher automobile emissions standards and be more environment friendly as the electrified vehicles have less pollution production. Furthermore, the electrified vehicle's powertrain can have an obvious efficiency improvement because of the regenerative capability, compared with the Internal Combustion Engine (ICE). In electrified vehicles, batteries, electric motors and power electronic converters are three important components. The electricity is stored in the battery, and to drive the motor, a power electronic converter is put in between to control the voltage and current input to the motor. Generally, the battery part is the most expensive part in an electric vehicle, thus the electric energy available in the car is very precious and the utilization of the energy should be considered carefully.

To improve the utilization of the energy in the battery, optimizing the efficiency of the motor part and the power electronic converter part are two possible solutions. Motor efficiency optimization methods have attracted lots of research interests for many years and there have been numerous studies presented the methods from motor type selection, motor design and control strategies point of view[1][2][3][4][5]. While for the power electronic part, the two level inverter has been used for decades and is by far the most commonly used topology in motor drive systems at present. Studies have been done to improve the performance of the inverter by replacing the semiconductor devices with the new silicon carbide type[6] [7][8]. However, this kind of method is highly dependent on the development of semiconductor devices. Recently, multilevel converters have gained more interest because of it is a technical way to improve the performance of a motor drive system. Compared with the two level inverter, the multilevel converter has several advantages. Besides the benefit of a higher efficiency, the improvement of voltage quality, reduction of stress on power switches (which makes it is possible to choose a lower voltage level switch) and possible increment lifespan of the battery are also very attractive[9][10].

The three level neutral-point-clamped (NPC) inverter is one of the most known multilevel

topologies and is widely used in high voltage areas and medium voltage drive systems. Some studies of a NPC inverter drive system for electric vehicles have shown that it is a suitable application with attractive performance[11][12][13]. However, a drawback of the NPC inverter is the unbalancing loss distribution among semiconductor devices[14][15]. The active version of the NPC inverter, by using switching devices to replace the clamp diodes in the NPC, has the possibility to solve the unequal loss distribution problem[16]. In [17], the losses analysis of the three-level active neutral-point-clamped (ANPC) converters in wind energy conversion application is presented. In [18], a brushless DC (BLDC) drive system with an ANPC inverter is implemented and the voltage and current THD and torque ripple performances are investigated. In [19], an electric vehicle conversion system based on a surface PMSM and ANPC inverter is proposed and investigated. However, a performance evaluation of the ANPC inverter in an electric vehicle drive system is missing. In this thesis, an ANPC inverter based drive system for an electric vehicle is developed and the efficiency performance of the inverter with various drive cycles are evaluated. Moreover, the efficiency as well as the voltage and current THD performances are compared with a two level inverter for a better understanding.

1.2 Purpose

The main purpose of this thesis is to investigate the performance of an electric drive system for an electric vehicle with an ANPC inverter and to conduct an efficiency and THD performance comparison with the conventional two level inverter.

1.3 Thesis Outline

In Chapter 2, basic theories of electric drive system are introduced including power electronics converters, PMSM modeling as well as different drive cycles. In Chapter 3, the operation principle of the ANPC inverter is studied carefully including the modulation strategy, modulation method and simulation results analysis. In Chapter 4, the performance of the ANPC inverter is evaluated. The voltage and current THD, the power losses and efficiency in various drive cycles of the ANPC inverter are compared with the two-level inverter. Moreover, the losses distribution of the ANPC inverter is studied. Finally, some conclusions and possible future work are listed in in Chapter 5 and 6.

2

Electric Drive System

2.1 Electric Drive System

The typical structure of an electric vehicle system is shown in Figure 2.1. The DC batteries supply electric power for the whole system. The power converter is used to control the voltage supplied to the motor and subsequently to control the torque and speed of the motor.

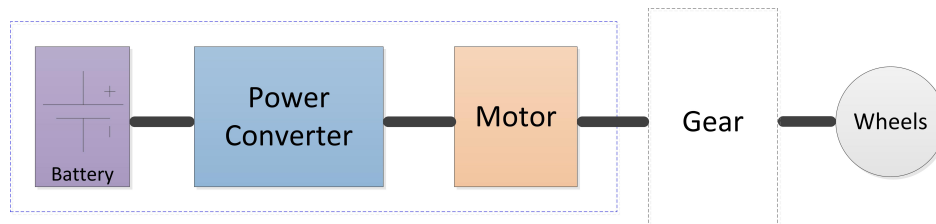


Figure 2.1: Drive system of a electric vehicle

2.2 Power Electronics Converters

In the motor drive system of electrified vehicles, two level inverters are the most widely used at present. To achieve a higher power for a higher speed application, one practical method is to increase the DC side voltage. When the power and DC side voltage is increased, a high power higher voltage converter is required. To implemented this inverter, one solution relies on the high power semiconductor devices. However, the higher power device will produce more losses and is usually more expensive. Besides the devices solution, there is another topological level solution known as the multilevel converter topology. As is shown in Figure 2.2, the two-level converter equals to a 2-pole 1 throw switch that can only be connected to positive and zero rail. In contrast, the multilevel converter in Figure 2.3 is equivalent to a multi-pole 1 throw switch that can generate multiple output voltage levels. For the multilevel converter, there will be more control freedom when synthesizing the output voltage. Besides, when the DC side voltage is fixed, voltage stress on each switch is less in multilevel converters and the lower power rating devices with low cost can be used to replace one high power rating device. Furthermore, each device is switched at lower voltage and has

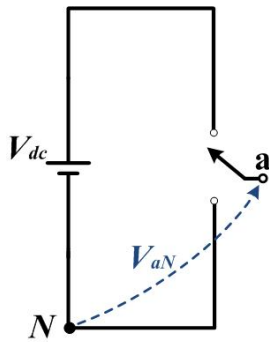


Figure 2.2: Two-level converter

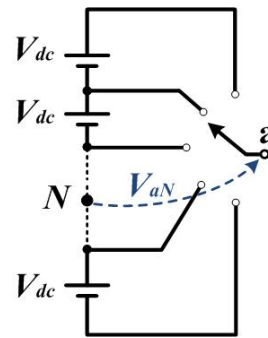


Figure 2.3: Multilevel converter

smaller dv/dt , hence the switching noise is reduced and the EMI issues can be improved. Moreover, as the multilevel output voltage synthesises the reference waveform in a better way compared to the two-level inverter, a better output power quality can be achieved.

2.2.1 Multilevel inverters

Because of the above mentioned benefits and advantages for multilevel converters, the topologies have been studied for decades and numerous variations have been invented. In general, the most commonly used topologies of multilevel converters are flying capacitor (FC) converter, the neutral point clamped (NPC) converter and the cascaded multilevel converter. Among all the multilevel converters, the three-level inverter is one of the most widely used topologies.

The diode neutral point clamped (DNPC) phase leg in Figure 2.4 (a) is the original NPC topology, which comprises two traditional two-level half bridge cells stacked together with two clamping diodes connected to the neutral point. By replacing the clamping diodes with active switches in Figure 2.4(b), the active neutral point clamped (ANPC) topology can be derived. The DNPC topology has uneven loss and stress distribution for each device on the phase leg. The ANPC topology can solve this problem by proper control strategy. One issue for the NPC topologies is the requirement of extra control for balancing the neutral point voltage. The three-level output voltage can also be generated by a floating capacitor as shown in Figure 2.4 (c), which is the flying capacitor (FC) topology. Although the FC circuit does not have the neutral point voltage balance problem, it still requires extra control to maintain the flying capacitor voltage at half the DC link voltage. The cascaded topology shown in Figure 2.4(d) is another widely used structure. The phase leg contains two basic two-level converter cells that are cascaded together. With this modularized structure, the output voltage can reach higher level by increasing the cell numbers. However, with voltage level increasing, more multiple isolated DC sources will be needed.

2.2.2 Modulation strategies

For modulation methods, there are two major groups, one is the space vector based and the other is carrier based. The SPWM method is the most commonly used carrier based method

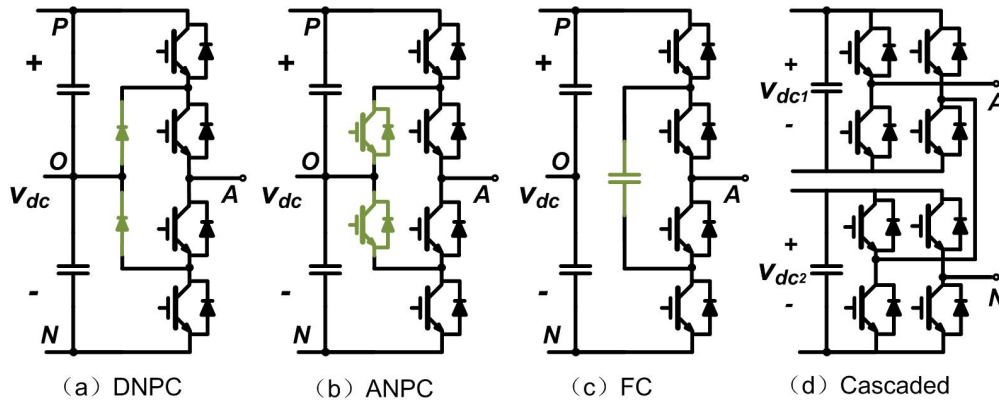


Figure 2.4: Topologies of 3-level inverters

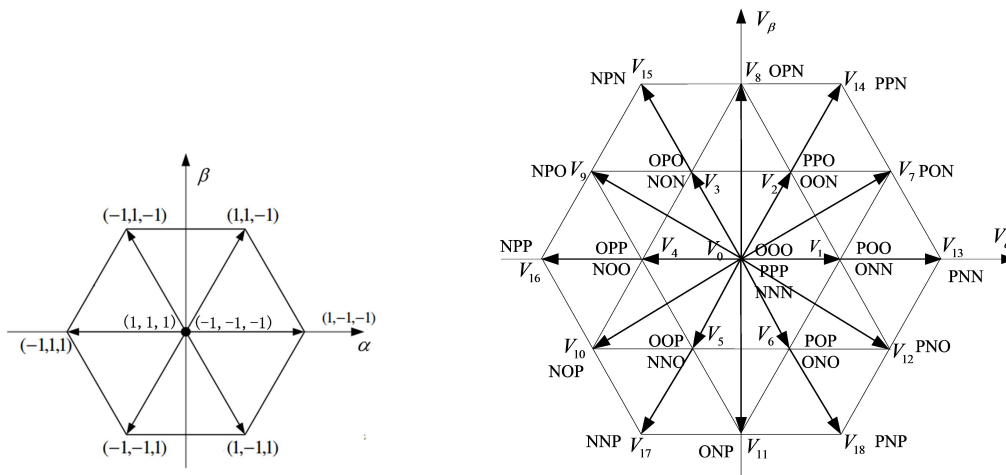


Figure 2.5: Space vector hexagon for 2-level and 3-level converter

in AC systems. While the SVM method is more widely used in three phase AC systems for its higher utilization of the DC voltage. For the space vector modulation, the voltage vectors in 3-phase abc coordinates transformed to $\alpha - \beta$ coordinates and all voltage vectors are mapped on the space vector hexagon. The switching status for the three-level converter can also be mapped on the hexagon. The voltage reference can be synthesized in various manners by the space vectors, or the switching status. For a two-level converter, each phase leg has 2 switching status and the 3-phase system has 8 switching statuses, corresponding to 7 space vectors in the space vector hexagon. While for a three-level converter, each phase leg has 3 switching status and the 3-phase system has 27 switching statuses, corresponding to 19 space vectors in the space vector hexagon. The space vector hexagons for 2-level and 3-level inverters are shown in Figure 2.5.

For multilevel converters, the number of switching status is the cube of the level numbers. The higher level numbers gives more redundant switching status for control freedom, but it also causes higher computation cost for the reference voltage locating. Therefore, the SVM will be hard to implemented when the number of levels goes too high. But for the three-level NPC topology, SVM is quite suitable since the calculation is not complex and there is control freedom to achieve neutral point voltage balancing.

2.2.3 Losses of semiconductor devices

The power losses produced by an IGBT module is shown in Figure 2.6. The IGBT and the free-wheeling diode have conduction losses and switching losses. The conduction losses occur when the current passes through the on-state voltage of the device while the switching losses is caused by the switching actions. The switching losses in the IGBT consist of the turn on loss and the turn off loss while the switching losses in the diode are caused by the reverse recovery.

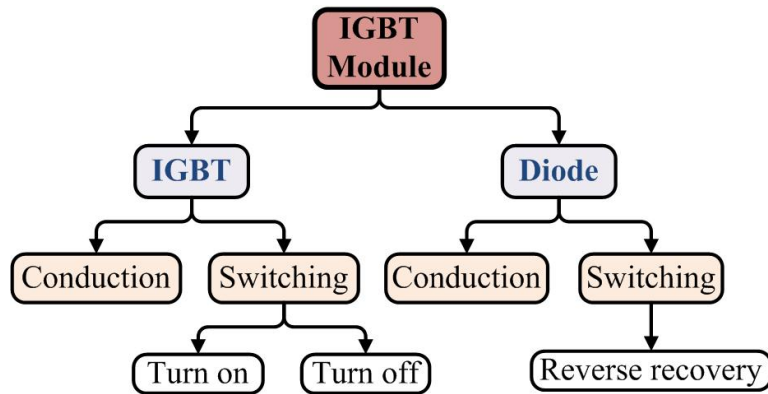


Figure 2.6: Losses of the IGBT module

2.2.3.1 Conduction losses

The conduction losses of the IGBT occur when it is conducting current. The average power dissipation during conduction in one switching period can be written as

$$P_{cond} = \frac{1}{T} \int_0^T v_{ce,sat} i_{ce} dt \quad (2.1)$$

where T is the switching period, $v_{ce,sat}$ and i_{ce} are the on-state voltage and current. The $v_{ce,sat}$ can be calculated as

$$v_{ce,sat} = V_{ce,0} + r_{on} i_{ce} \quad (2.2)$$

where $V_{ce,0}$ is the saturation voltage at zero current and r_{on} is the on-state resistance. These two values can be obtained from the output characteristic of the IGBT, as is shown in Figure 2.7. r_{on} can be derived by

$$r_{on} = \frac{\Delta V_{ce}}{\Delta I_c} \quad (2.3)$$

For the conduction losses of the diode, the calculation method is similar.

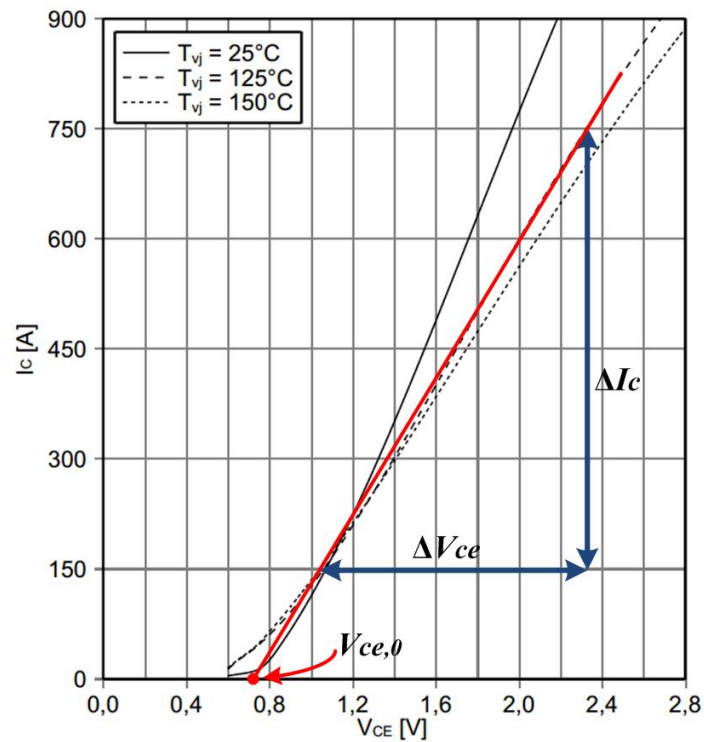


Figure 2.7: Output characteristic of the IGBT [20]

2.2.3.2 Switching losses

To analyse the switching losses of semiconductor devices, the switching waveforms should be considered first. Figure 2.8 shows the turn on waveforms of an IGBT with free-wheeling diode. When the IGBT is turned on, the diode will turn off. The peak current I_{rr} is caused by the reverse recovery of the diode.

The turn on energy loss of the IGBT can be calculated as

$$E_{on} = \int_{t_0}^{t_2} v_{ce} i_{ce} dt = \int_{t_0}^{t_2} P_{sw} dt \quad (2.4)$$

For the diode, the turn off loss only occurs when its voltage and current are not zero, thus the turn off loss is

$$E_{rr} = \int_{t_1}^{t_2} v_{ce} i_f dt = \int_{t_1}^{t_2} P_{diode} dt \quad (2.5)$$

The turn off waveform of the IGBT with free-wheeling diode is similar but the diode has no losses during this process. Therefore, the switching losses in one IGBT module consist turn on loss E_{on} and turn off loss E_{off} of the IGBT as well as the reverse recovery loss E_{rr} of the diode.

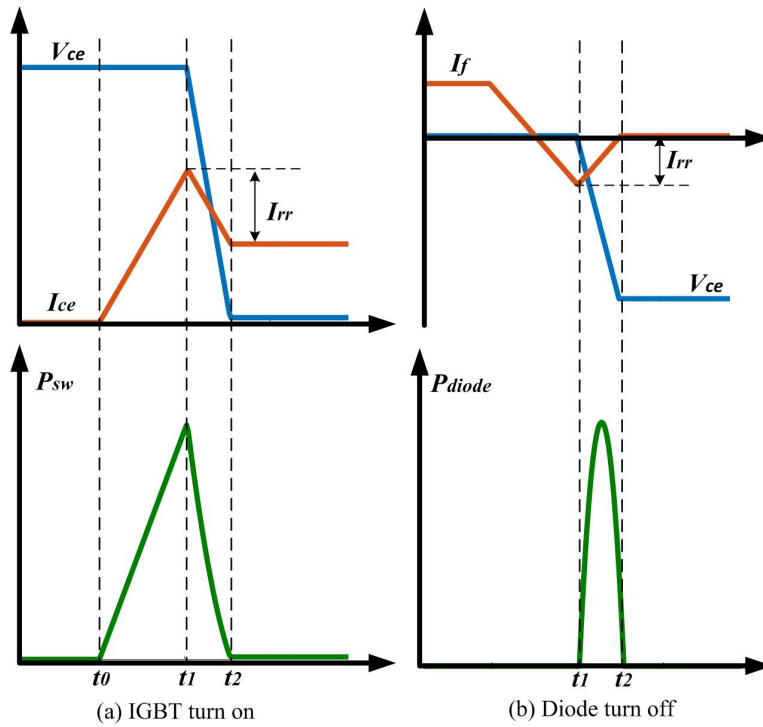


Figure 2.8: Switching curves for IGBT with free-wheeling diode

Usually, in the datasheet of the semiconductor device, it only shows the switching energy loss for a specific voltage and current. For other voltages and currents, the switching energy loss can be predicted as

$$E_{on} = E_{on,ref} \left(\frac{v_{ce}}{V_{ce,ref}} \right)^{k_{v,on}} \left(\frac{i_{ce}}{I_{ce,ref}} \right)^{k_{i,on}} \quad (2.6)$$

$$E_{rr} = E_{rr,ref} \left(\frac{v_{ce}}{V_{ce,ref}} \right)^{k_{v,rr}} \left(\frac{i_{ce}}{I_{ce,ref}} \right)^{k_{i,rr}} \quad (2.7)$$

$$E_{off} = E_{off,ref} \left(\frac{v_{ce}}{V_{ce,ref}} \right)^{k_{v,off}} \left(\frac{i_{ce}}{I_{ce,ref}} \right)^{k_{i,off}} \quad (2.8)$$

where $V_{ce,ref}$ and $I_{ce,ref}$ are the reference voltage and current, $E_{on,ref}$, $E_{rr,ref}$ and $E_{off,ref}$ are the switching energy losses at the reference value, $k_{v,on}$, $k_{i,on}$, $k_{v,rr}$, $k_{i,rr}$, $k_{v,off}$ and $k_{i,off}$ are coefficients which relate the energy losses at the reference value to other values. The $E_{on,ref}$, $E_{rr,ref}$ and $E_{off,ref}$ values can find in the datasheet directly while the coefficients usually need to be derived from the characteristic figures of the device.

2.3 PMSM Modeling

For the three phase motors, analysis in $d-q$ coordinate system is usually more convenient than in abc coordinate system. Meanwhile, as the dynamic behavior is not of interest for

losses analysis, the steady state model is sufficient in our case. In steady state, the terminal voltages of the PMSM machine can be written as a function of terminal currents as

$$\begin{cases} U_{sd} = R_s I_{sd} - \omega_e L_q I_{sq} \\ U_{sq} = R_s I_{sq} + \omega_e L_d I_{sd} + \omega_e \psi_m \end{cases} \quad (2.9)$$

where R_s is the stator resistance, ω_e is the electrical angular speed, L_d and L_q are the equivalent inductance in d,q axis respectively and ψ_m is the permanent magnet flux density.

If L_d and L_q are equal, the electric torque of the motor is formed as

$$T_e = \frac{3}{2} n_p \psi_m I_{sq} \quad (2.10)$$

2.4 Drive Cycles

The ECE is a urban driving cycle and it is designed to represent typical driving conditions in European cities. As is shown in Figure 2.9, during this driving cycle, the driving speed is relatively low and there are many braking and accelerating. EUDC is the extra urban driving cycle and it is designed to to represent a high speed driving mode. Figure 2.10 shows that the speed during one cycle is high and the maximum speed can reach 120 km/h.

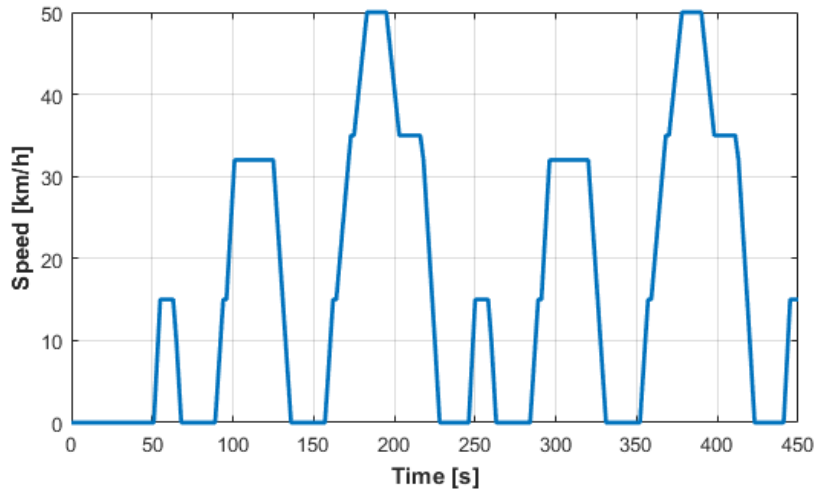


Figure 2.9: Drive cycle ECE

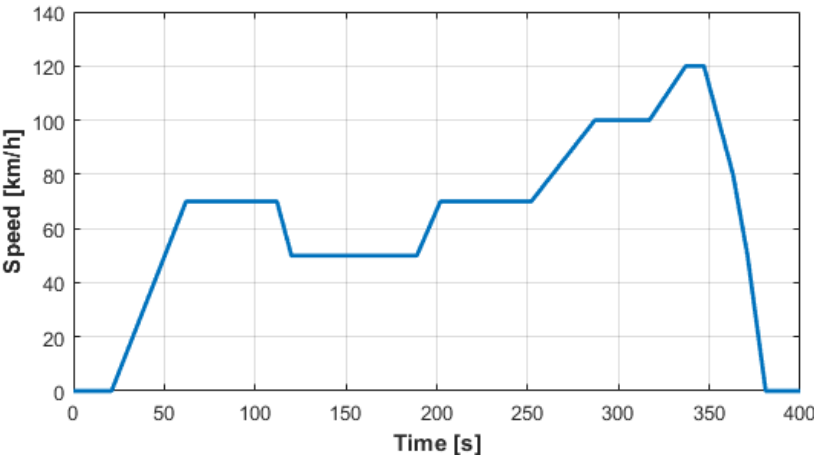


Figure 2.10: Drive cycle EUDC

3

Operation Principle of the ANPC Inverter

In this chapter, an ANPC inverter is introduced. The operation principle of the inverter is analyzed and a SVM modulation method is used to control the inverter. A two-level inverter is introduced at the end to provide a performance comparison for the ANPC inverter.

3.1 Modulation Strategy of ANPC Inverter

The basis topology of an ANPC inverter is shown in Figure 3.1. It can be seen that for each phase there are two additional active switches anti-parallelled with the clamping diodes. Since the modulation strategy is the same for each phase, analysis on one phase leg is sufficient.

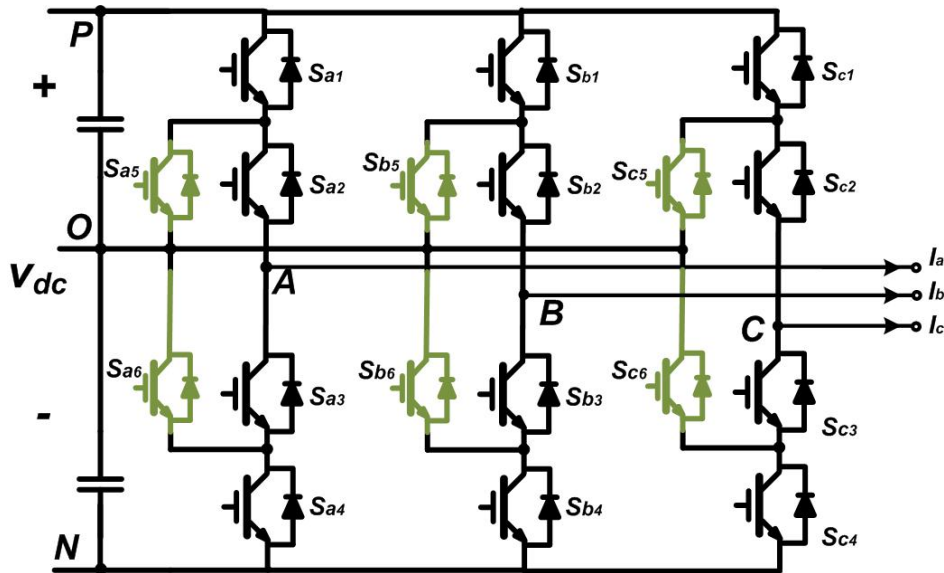


Figure 3.1: Structure of ANPC inverter

For one phase, the relation of switching states and the output voltage is shown in Table 3.1. The output voltage has three values: $V_{dc}/2$, $-V_{dc}/2$ and 0. For negative and positive voltage level there is only one switching state, N for negative and P for positive respectively. While

for the zero voltage level, there are two switching states: O^- and O^+ . When the reference voltage is negative, O^- is obtained with S_2 , S_4 and S_5 turned on while S_1 , S_3 and S_6 is turned off. When the reference voltage is positive, O^+ is obtained with turning on and off switches opposite to O^- . For O^- and O^+ states, the load current can flow through S_2 and S_5 or only through S_3 and S_6 in both directions.

Table 3.1: Switching sequence of ANPC inverter

Output voltage (v_{Ao})	Switching states	S_1	S_2	S_3	S_4	S_5	S_6
$-V_{dc}/2$	N	0	0	1	1	1	0
0	O^-	0	1	0	1	1	0
	O^+	1	0	1	0	0	1
$V_{dc}/2$	P	1	1	0	0	0	1

Figure 3.2 shows the gate signal waveforms of the six switches. The outer switches S_1 and S_4 and the clamping switches S_5 and S_6 are complimentary, and they operate with the reference voltage frequency. Meanwhile, the 2 complimentary inner switches have high switching frequency over the whole period. The current paths for different states changing are shown in Figure 3.3. The switching loss only occurs on the inner switches regardless of the power factor.

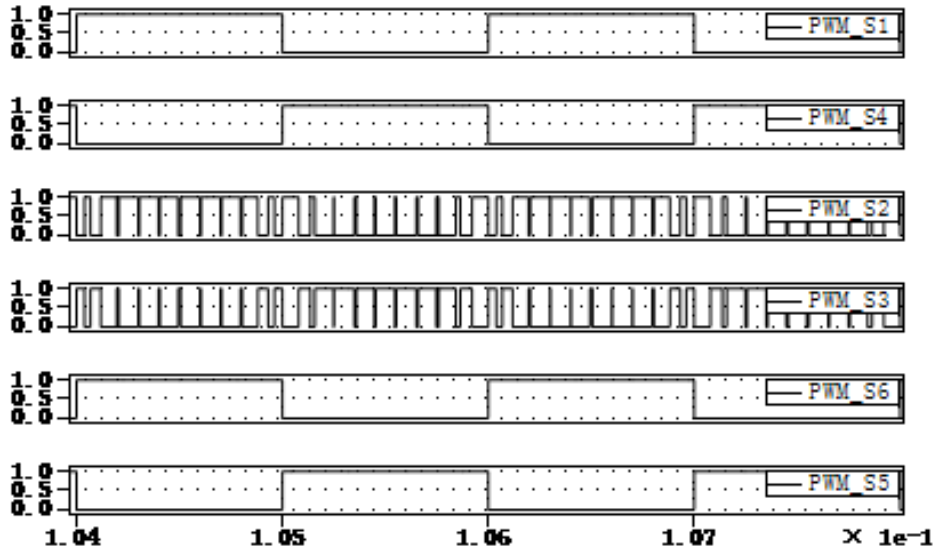


Figure 3.2: Gate signals

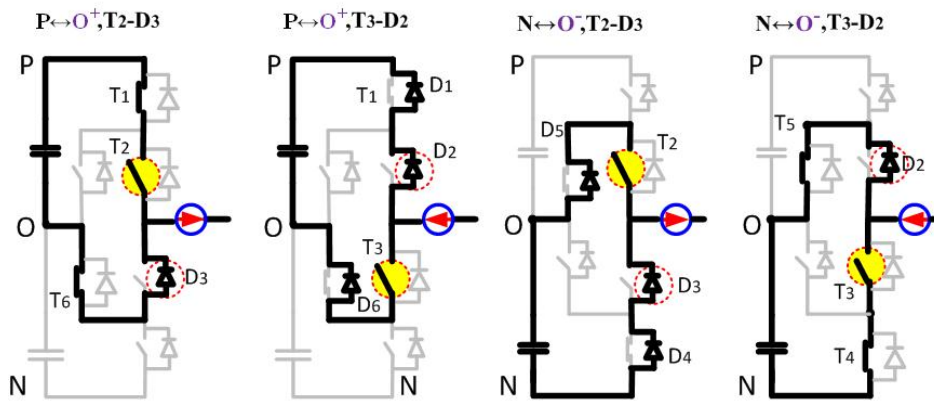


Figure 3.3: Current path for states changing

3.2 SVM Method of ANPC Inverter

3.2.1 Space vector diagram of ANPC inverter

The space vector diagram of the ANPC inverter is shown in Figure 3.4. For the simplification of the diagram analysis, both O^- and O^+ are represent by O and considered to be the same switching state. Each phase of the ANPC converter has three sates: P , N and O . Thus there are a total of $3^3 = 27$ switching states, corresponding to 19 space vectors in the space vector hexagon. There are six long vectors, six medium vectors, six small vectors, and one zero vector. Each long vector and medium corresponds to one switching state, each small vector corresponds two switching states and the zero vector corresponds to 3 switching states.

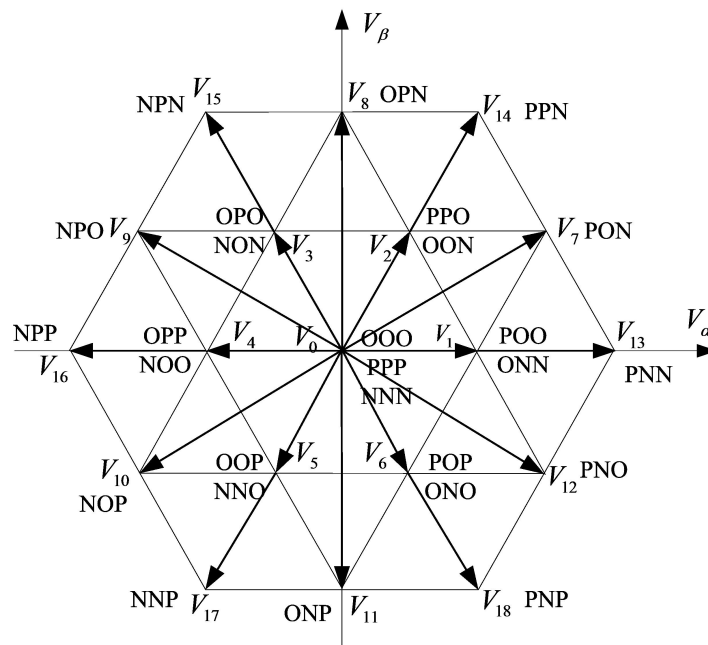


Figure 3.4: Space vector diagram.

3.2.2 Sector identification

For the SVM method, the space vectors are in $\alpha - \beta$ coordinates thus a transformation from abc coordinates to $\alpha - \beta$ coordinates should be done at first. The transformation can be done by using the Clark transformation matrix,

$$\begin{bmatrix} u_\alpha \\ u_\beta \end{bmatrix} = \frac{2}{3} \begin{bmatrix} 1 & -\frac{1}{2} & -\frac{1}{2} \\ 0 & -\frac{\sqrt{3}}{2} & \frac{\sqrt{3}}{2} \end{bmatrix} \begin{bmatrix} u_a \\ u_b \\ u_c \end{bmatrix} = \begin{bmatrix} u_m \cos \theta \\ u_m \sin \theta \end{bmatrix} \quad (3.1)$$

where u_m is the voltage magnitude in $\alpha - \beta$ coordinates and θ is the angle between the voltage vector and the α axis.

3.2.2.1 Large sector identification

Similarly to the two level inverter, the ANPC inverter space vector diagram can also be divided into six sectors and each sector has a width of 60 degree.

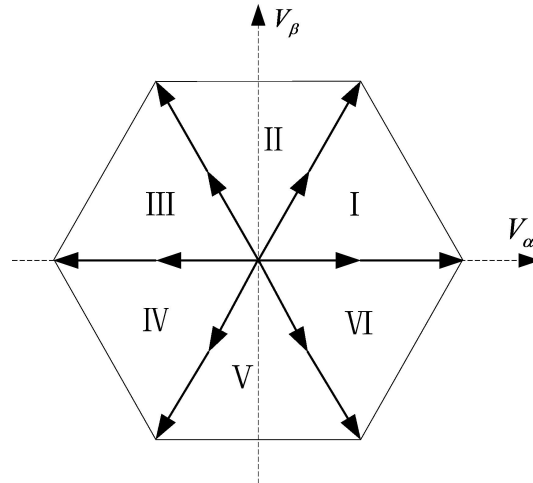


Figure 3.5: Six-sector division diagram.

The sector which the reference voltage is located can be identified according to the criterion below: Define three variables A, B, C and three values as

$$\begin{aligned} U_{ref1} &= u_\beta \\ U_{ref2} &= \sqrt{3}u_\alpha - u_\beta \\ U_{ref3} &= -\sqrt{3}u_\alpha - u_\beta \end{aligned} \quad (3.2)$$

If $U_{ref1} > 0$, $A = 1$, if not $A = 0$;

If $U_{ref2} > 0$, $B = 1$, if not $B = 0$;

If $U_{ref3} > 0$, $C = 1$, if not $C = 0$.

Define $N = 4C + 2B + A$, then the values of N have a relation with the number of sectors as shown in Table 3.2.

Table 3.2: Sector identification table

N	3	1	5	4	6	2
Sector	I	II	III	IV	V	VI

3.2.2.2 Sub-sector identification

When the sector of the reference voltage is identified, the location of reference voltage is in which sub-sector need to be determined. In the space vector diagram, each sector is divided into four sub-sectors. Taking Sector I as an example, it is divided into four triangular shaped sub-sectors named as A, B, C and D , as is shown in Figure 3.6.

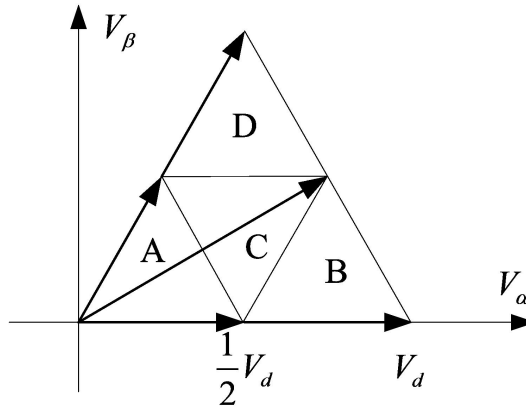


Figure 3.6: Sub-sector division diagram in Sector I.

The sub-sectors can be identified according to the criterion below: Define three variables A, B, C and three values as

$$U_{re1} = u_\beta - \frac{\sqrt{3}}{4}.$$

$$U_{re2} = \frac{1}{2} - u_\alpha - \frac{1}{\sqrt{3}}u_\beta.$$

$$U_{re3} = u_\alpha - \frac{1}{2} - \frac{1}{\sqrt{3}}u_\beta.$$

If $U_{re1} > 0$, $A = 1$, if not $A = 0$.

If $U_{re2} > 0$, $B = 1$, if not $B = 0$.

If $U_{re3} > 0$, $C = 1$, if not $C = 0$.

Define $SN = 3C + 2B + A$, then the values of SN have a relation with the number of sectors as shown in Table 3.3.

Table 3.3: Subsector identification table

SN	2	3	0	1
Subsector	A	B	C	D

If the reference vector is not located in Sector I, u_α and u_β can be transformed to u_α' and u_β' and then the principle discussed above can be used directly. For different sectors, the transformation equation is shown in table below.

Sector	u_α'	u_β'
I	u_α	u_β
II	$\frac{1}{2}u_\alpha + \frac{\sqrt{3}}{2}u_\beta$	$\frac{1}{2}u_\beta - \frac{\sqrt{3}}{2}u_\alpha$
III	$-\frac{1}{2}u_\alpha + \frac{\sqrt{3}}{2}u_\beta$	$-\frac{1}{2}u_\beta - \frac{\sqrt{3}}{2}u_\alpha$
IV	$-u_\alpha$	$-u_\beta$
V	$-\frac{1}{2}u_\alpha - \frac{\sqrt{3}}{2}u_\beta$	$-\frac{1}{2}u_\beta + \frac{\sqrt{3}}{2}u_\alpha$
VI	$\frac{1}{2}u_\alpha - \frac{\sqrt{3}}{2}u_\beta$	$\frac{1}{2}u_\beta + \frac{\sqrt{3}}{2}u_\alpha$

3.2.3 Vector turn-on time calculation

With the SVM method, the reference voltage vector can be expressed as the sum of three of the voltage vectors. For each of these voltages, the amplitude is set as a function of the turn-on time. Therefore

$$V_r T = V_1 t_1 + V_2 t_2 + V_3 t_3 \quad (3.3)$$

where V_r is the reference voltage vector, T is the switching frequency, V_1, V_2, V_3 are three vectors in the space diagram and t_1, t_2, t_3 are the turn on time corresponding to V_1, V_2, V_3 . And $t_1 + t_2 + t_3 = T$.

Let us take a case from Figure 3.7, where a reference voltage vector is in sector I, sub-sector A. The reference voltage vector can be expressed as

$$V_r T = V_0 t_0 + V_1 t_1 + V_2 t_2 \quad (3.4)$$

Moreover, with the expression

$$t_0 + t_1 + t_2 = T \quad (3.5)$$

Equation (3.4) can be rewritten in the α and β axis respectively

$$\begin{cases} u_{\alpha}T = V_0t_0 + V_1t_1 \cos 0^{\circ} + V_2t_2 \cos 60^{\circ} \\ u_{\beta}T = V_0t_0 + V_1t_1 \sin 0^{\circ} + V_2t_2 \sin 60^{\circ} \end{cases} \quad (3.6)$$

Suppose that the length of the large vector is V_d , thus the length of the small vector is half of V_d . With further calculations, t_0, t_1, t_2 can be expressed as

$$\begin{cases} t_0 = T - \frac{2T}{V_d} \left(u_{\alpha} + \frac{u_{\beta}}{\sqrt{3}} \right) \\ t_1 = \frac{2T}{V_d} \left(u_{\alpha} - \frac{u_{\beta}}{\sqrt{3}} \right) \\ t_2 = \frac{4u_{\beta}T}{\sqrt{3}V_d} \end{cases} \quad (3.7)$$

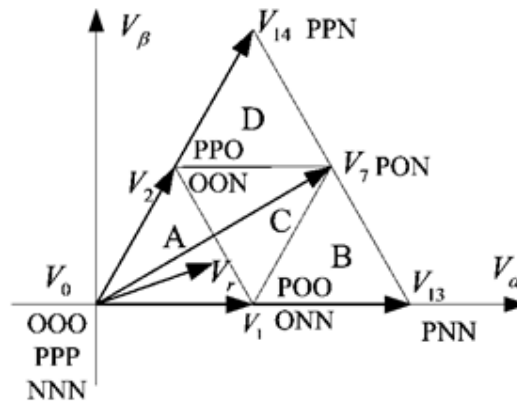


Figure 3.7: Vectors in sector I.

In other sectors and sub-sectors, we can use the same method to calculate turn-on time for each vector. And from the calculated results, we observe that there are some parts with same expressions, so we define the same parts as

$$\begin{cases} X = \frac{4u_{\beta}T}{\sqrt{3}V_d} \\ Y = \frac{2T}{V_d} \left(u_{\alpha} + \frac{u_{\beta}}{\sqrt{3}} \right) \\ Z = \frac{2T}{V_d} \left(u_{\alpha} - \frac{u_{\beta}}{\sqrt{3}} \right) \end{cases} \quad (3.8)$$

With (3.8), the turn on time of every space vector in different sub-sectors of sector I are shown in the Table 3.4. For other sectors, the calculations are similar.

3.2.4 Vector operation sequence

With the turn on time of each vector determined, the vector operating sequence needs to be considered. The principle to set the sequence is minimum switching actions. By dividing the

Table 3.4: Turn on time in Sector I

Sector I			
Sub-sector	Vector1	Vector2	Vector3
A	$t_0 = T - Y$	$t_1 = Z$	$t_2 = X$
B	$t_1 = 2T - Y$	$t_7 = X$	$t_{13} = -T + Z$
C	$t_1 = T - X$	$t_2 = T - Z$	$t_7 = -T + Y$
D	$t_2 = 2T - Y$	$t_7 = Z$	$t_{14} = X - T$

whole switching period into seven segments, the switching patterns in sector I, sub-sector A are shown in Figure 3.8

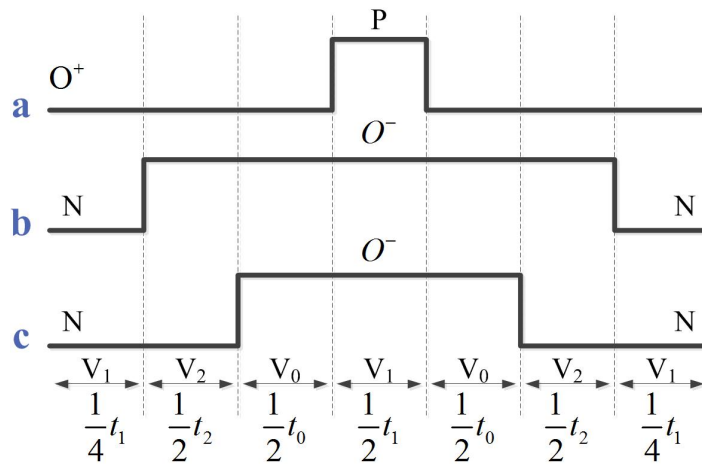


Figure 3.8: Vector patterns in sector A

With the same method, we can obtain the switching patterns of all sectors and sub-sectors. The vector sequence for each sub-sector in sector I is shown in the Table 3.5 as an example.

Table 3.5: Vector sequence in Sector I

Sector I	
Sub-sector	Vector Sequence
A	$ONN \rightarrow OON \rightarrow OOO \rightarrow POO \rightarrow OOO \rightarrow OON \rightarrow ONN$
B	$ONN \rightarrow PNN \rightarrow PON \rightarrow POO \rightarrow PON \rightarrow PNN \rightarrow ONN$
C	$ONN \rightarrow OON \rightarrow PON \rightarrow POO \rightarrow PON \rightarrow OON \rightarrow ONN$
D	$OON \rightarrow PON \rightarrow PPN \rightarrow PPO \rightarrow PPN \rightarrow PON \rightarrow OON$

3.3 Simulation Results

A simulation model is built in Matlab Simulink to test the function of the ANPC inverter. The DC voltage is set to 800V, the switching frequency is set to 10kHz and the load for the test is an RL load. The modulation waveforms with different modulation indexes are shown in Figure 3.9, 3.10 and 3.11.

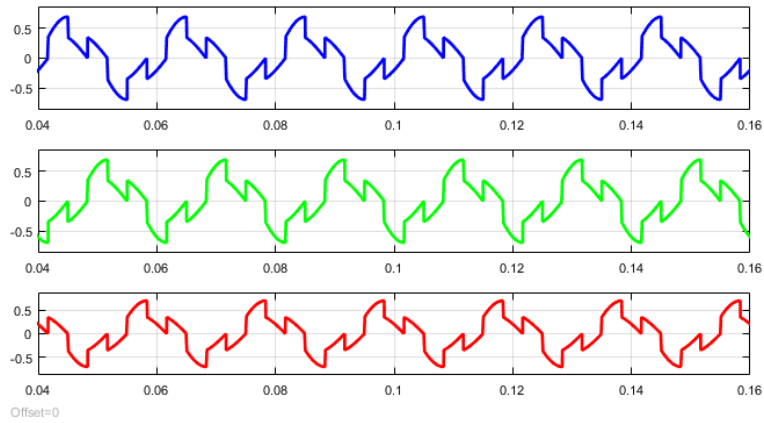


Figure 3.9: Modulation waveform with $m_a = 0.4$

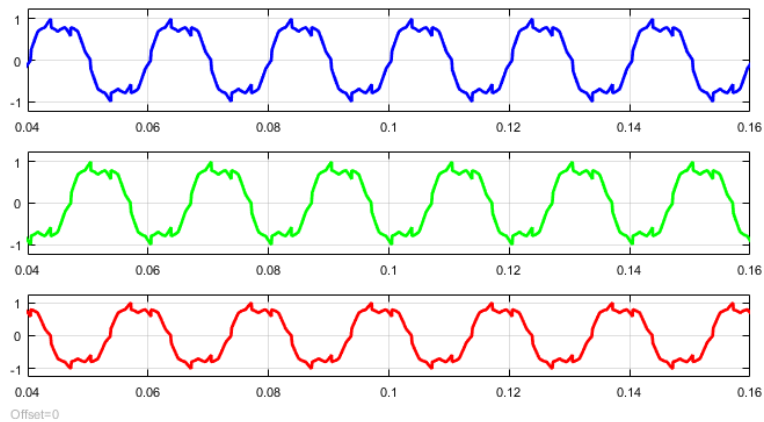


Figure 3.10: Modulation waveform with $m_a = 0.8$

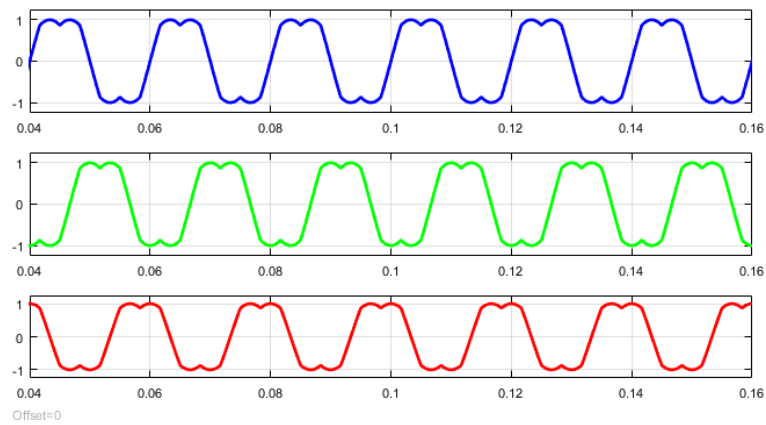


Figure 3.11: Modulation waveform with $m_a = 1$

The output line voltage and current waveforms at $m_a = 1$ are shown in Figures 3.12 and 3.13. And the FFT analysis of the voltage and current waveform are shown in Figures 3.14 and 3.15.

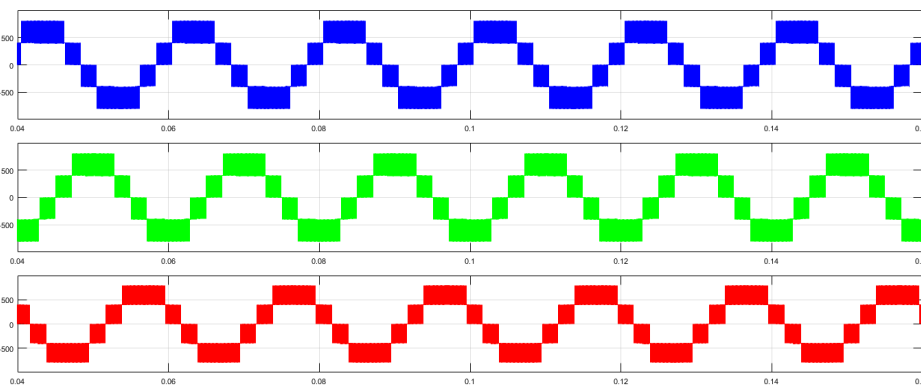


Figure 3.12: Line to line output voltage with $m_a = 1$

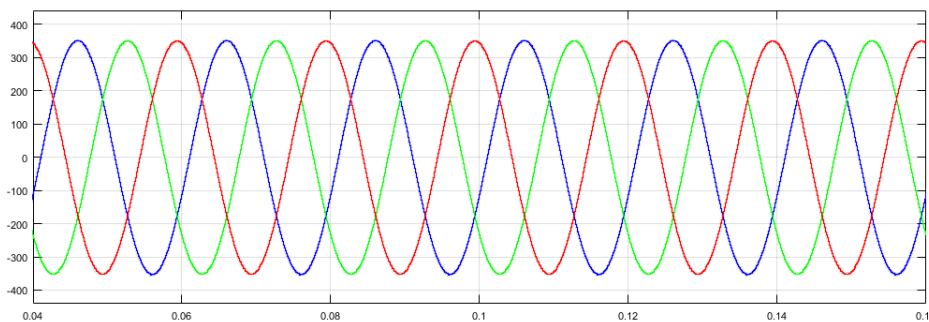


Figure 3.13: Output current with $m_a = 1$

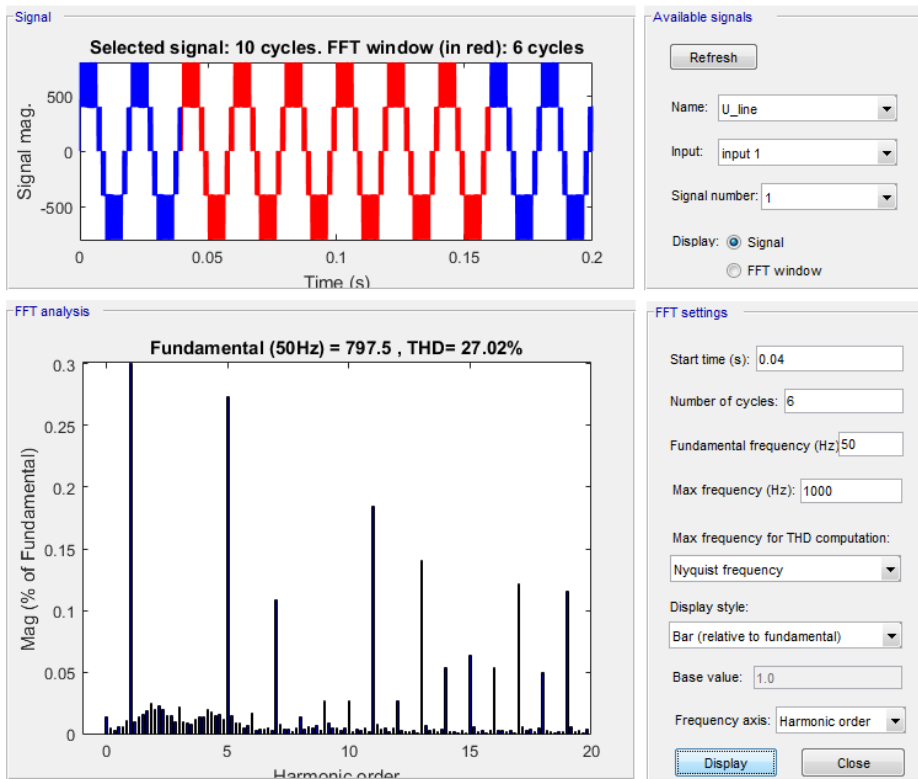


Figure 3.14: Harmonics analysis of line to line voltage with $m_a = 1$

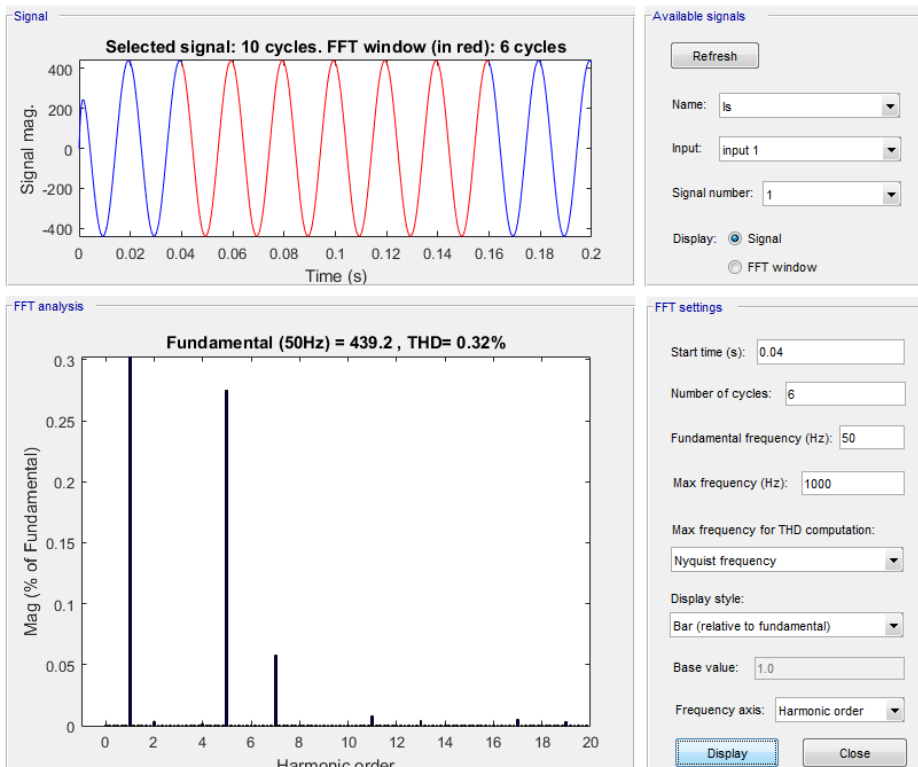


Figure 3.15: Harmonics analysis of output current with $m_a = 1$

3.4 Implementation of Two Level Inverter

To relate the results of the three-level ANPC inverter, a two level inverter is built for comparison. Similar to the ANPC inverter, the SVM modulation method is used in the two level inverter. The modulation waveform of the two level inverter when $m_a = 1$ is shown in Figure 3.16. The output line to line voltage and current are shown in Figure 3.17 and Figure 3.18 respectively. And the FFT analysis of the voltage and current waveform are shown in Figure 3.19 and 3.20.

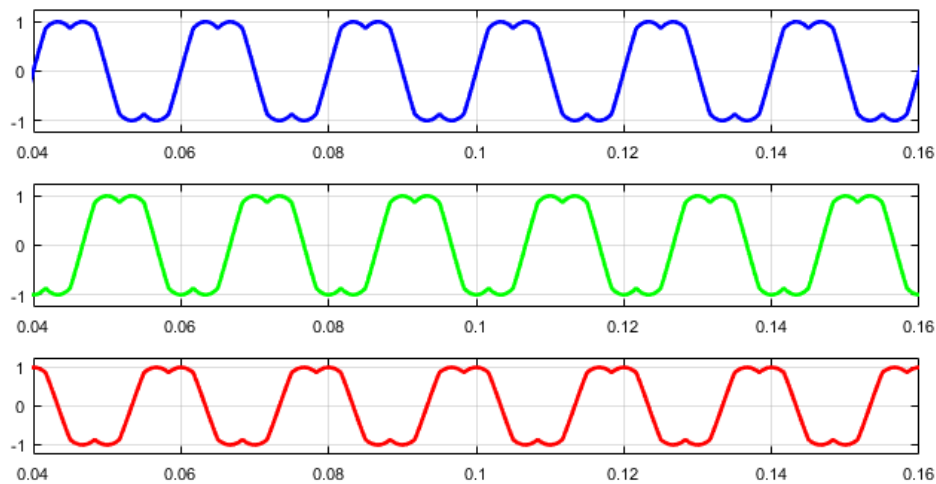


Figure 3.16: Modulation waveform with $m_a = 1$

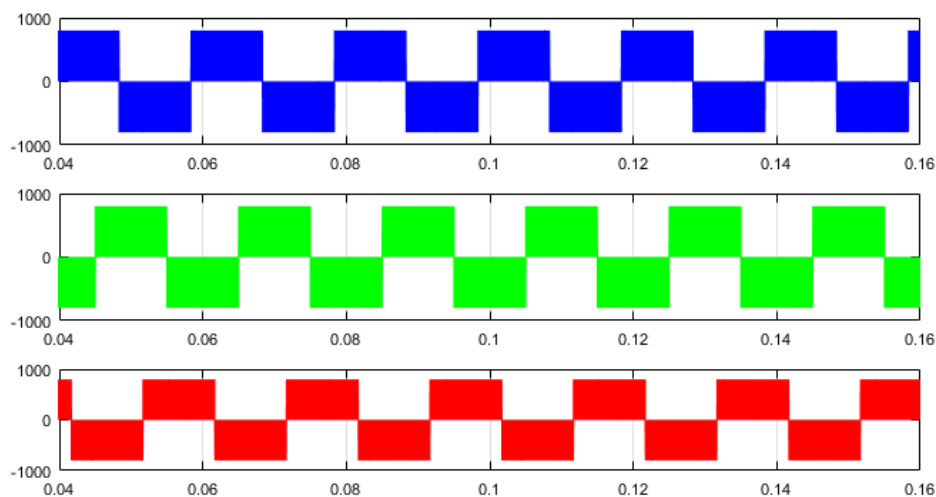


Figure 3.17: Line to line output voltage with $m_a = 1$

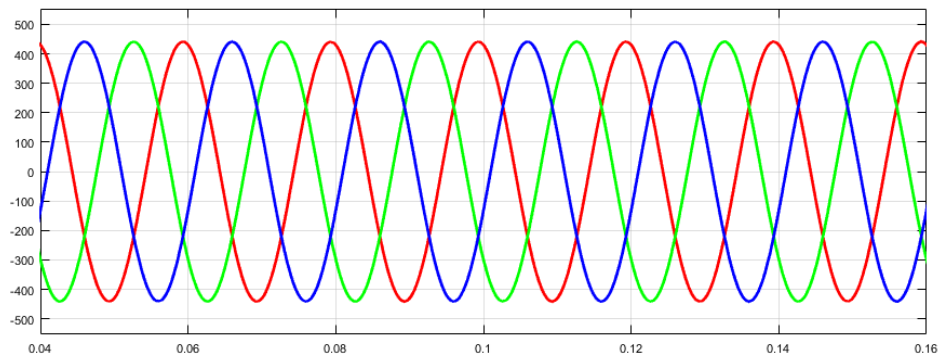


Figure 3.18: Output current with $m_a = 1$

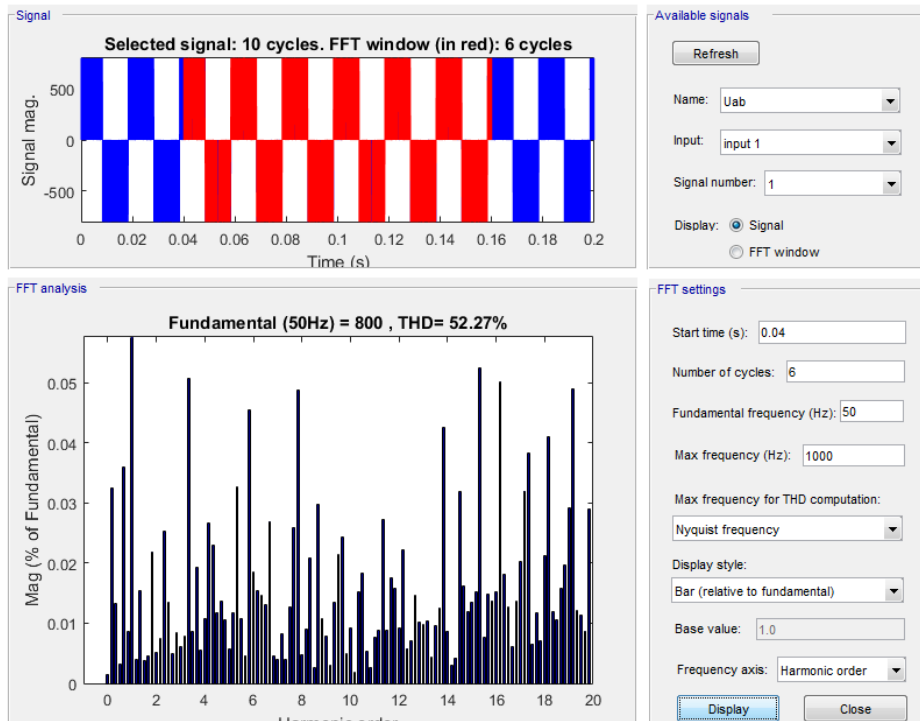


Figure 3.19: Harmonics analysis of line to line voltage with $m_a = 1$

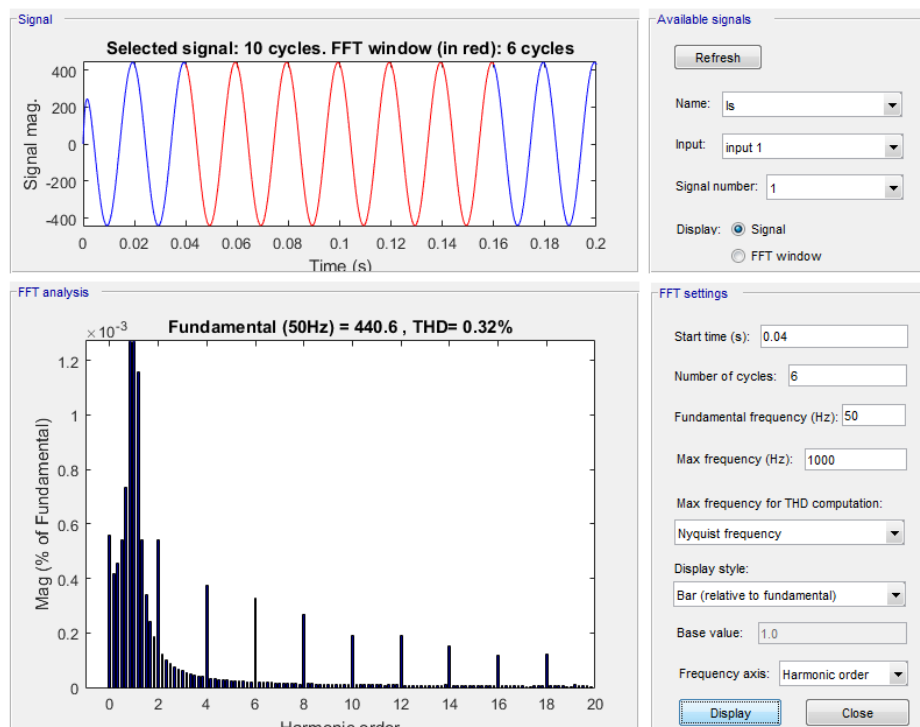


Figure 3.20: Harmonics analysis of output current with $m_a = 1$

4

Performance Evaluation of the ANPC Inverter

4.1 Case Setup

To evaluate the performance of the ANPC inverter in the electrified vehicle, the parameters of necessary components in a vehicle are determined. The electric machine used in the vehicle is a PMSM machine and its parameters are shown in Table 4.1. The needed electric parameters to simulate the inverter are shown in Table 4.2. The parameters of the car are shown in Table 4.3.

Table 4.1: Machine parameters

Parameter	Value
R_s	0.049 Ω
L_{sd}	2.28 mH
L_{sq}	2.28 mH
Ψ_m	0.26
p	2
U_{max} (phase voltage)	800/ $\sqrt{3}$ V
I_{max}	190 A

Table 4.2: Inverter parameters

Parameter	Value
V_{dc}	800 V
P_{rated}	125 kW
$U_{linemax}$	800 V
f_{switch}	10k Hz

Table 4.3: Vehicle Parameters

Curb weight	Cd	A	Cr	Tire radius
1650 kg	0.31	2.37 m ²	0.009	0.3284 m

4.1.1 Voltage and current requirement of the electric machine

In the drive system, the inverter is used to provide electric power to the electric machine. Thus the output voltage and current of the inverter should meet the requirement of the electric machine. For the electric machine, the voltage and current are related to the speed and the

torque. The torque, speed and voltage characteristics of the electric machine are shown in Figure 4.1 and the torque, speed and current magnitude characteristics are shown in Figure 4.2. As is shown in Figure 4.1, the voltage magnitude is increasing with the speed in the area below 8000 rpm. While in the relative high speed area, the voltage magnitude is kept almost constant. The reason is that, the possible voltage for the electric machine hits the limit of the inverter in this area. Thus the output voltage of the inverter can not increase any more. To ensure the normal operation of the electric machine in this area, the field weakening method is used. As is shown in Figure 4.2, the current magnitude increases almost linearly with the torque in the low speed area. While in the high speed area, because of the field weakening, the current magnitude have an obvious increment.

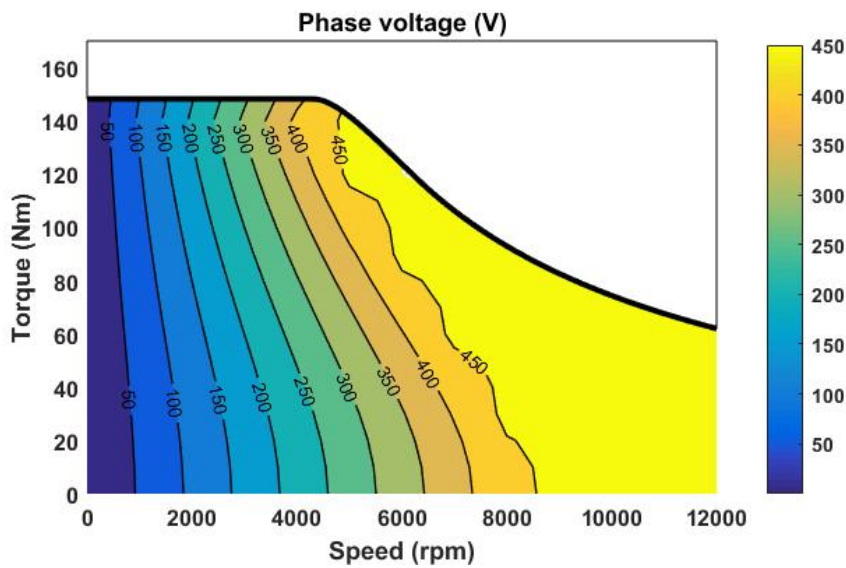


Figure 4.1: Required phase voltage magnitudes of the electric machine

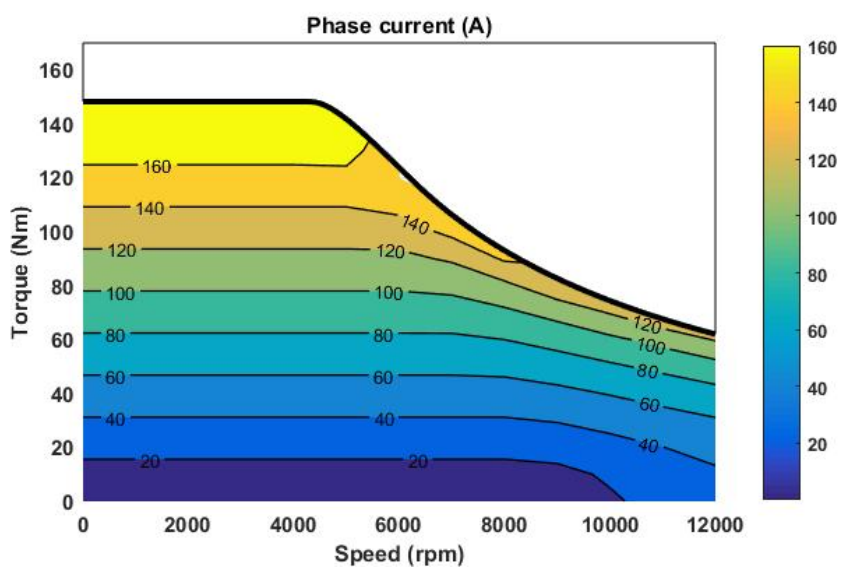


Figure 4.2: Required phase current magnitudes of the electric machine

4.2 Performance Comparison between the Two-level and the ANPC Inverter

As the two-level inverter is the most widely used inverter in electrified vehicles, to investigate the performance of the ANPC inverter, a comparison with the two-level inverter is worthwhile. To drive the electric machine mentioned above, an ANPC inverter model and a two-level inverter model are implemented in MATLAB separately. To evaluate the power losses of the inverter, the IGBT module *FF450R07ME4 – B11* is chosen for the ANPC inverter model [20]. With the same DC voltage requirement, the semiconductor device in the two-level inverter should be able to withstand a voltage twice of that in the ANPC inverter. Thus the IGBT module *FF450R12ME4 – B11* is chosen for the two-level inverter model [21]. The typical characteristic of the two IGBT models are shown in Table 4.4.

Table 4.4: IGBT characteristics based on datasheet and calculations

IGBTFF450R07ME4 – B11			IGBTFF450R12ME4 – B11		
$V_{CES} = 650 V$			$V_{CES} = 1200 V$		
@450 A, 300 V, 125°C			@450 A, 300 V, 125°C		
Parameters	IGBT	Diode	Parameters	IGBT	Diode
$V_{CE,0}$	0.65 V	0.8 V	$V_{CE,0}$	0.8 V	0.7 V
E_{on}	4.6 mJ		E_{on}	26 mJ	
E_{off}	28.5 mJ	8.9 mJ	E_{off}	55.5 mJ	48.5 mJ
R_{on}	2.33 mΩ	1.89 mΩ	R_{on}	2.78 mΩ	2.33 mΩ

4.2.1 Voltage and Current Comparison

The voltage THD characteristics of the two-level inverter and the ANPC inverter are shown in Figures 4.3 and 4.4. They show that the three level ANPC inverter has a smaller voltage distortion in the entire region. This is because the ANPC inverter has three levels of output voltage which can synthesis the reference voltage in a better way. The results show that the maximum voltage THD reduction is as much as 101 %. The current THD of the two inverters are shown in Figures 4.5 and 4.6. Both of the two inverters have low THD distortion. This is because the PMSM can be equivalent to an RL load with a back EMF, thus the output current harmonics of the inverters will be filtered. Figures 4.5 and 4.6 also show that the current THD of the ANPC inverter is lower than the two-level inverter and the maximum reduction can be 1.3 %.

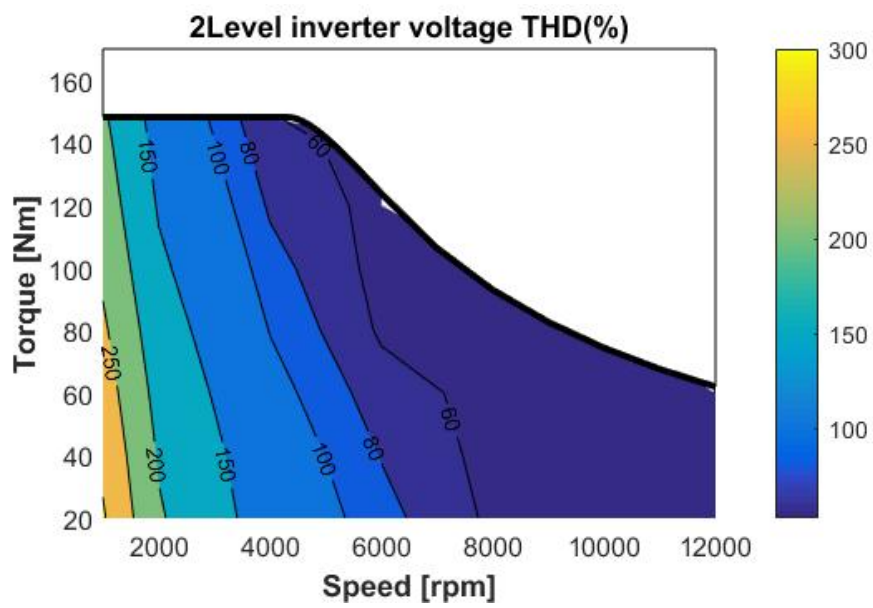


Figure 4.3: Phase voltage THD of the two-level inverter

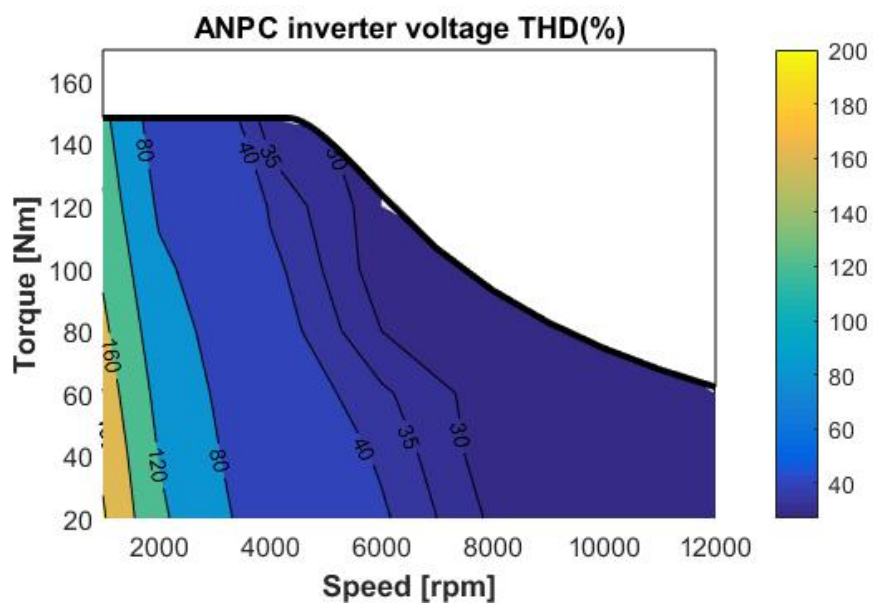


Figure 4.4: Phase voltage THD of the ANPC inverter

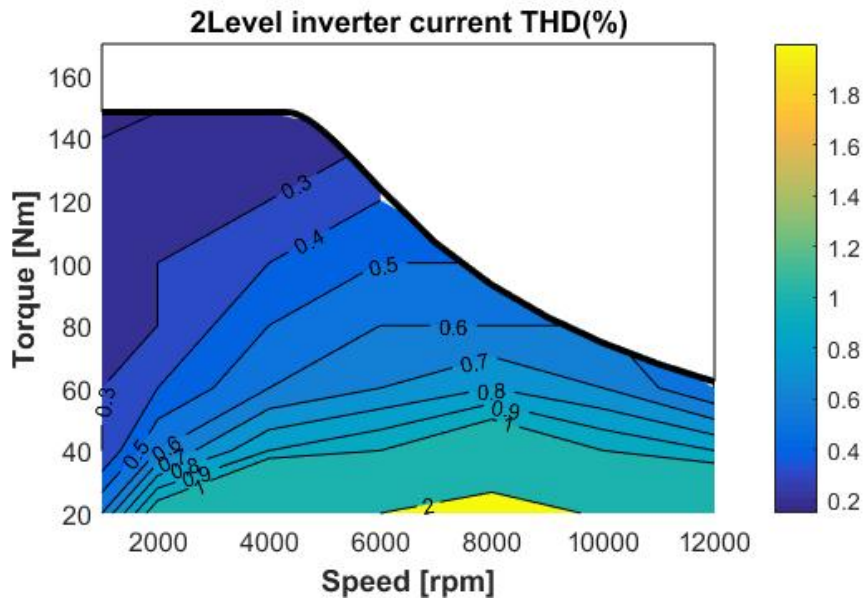


Figure 4.5: Current THD of the two-level inverter

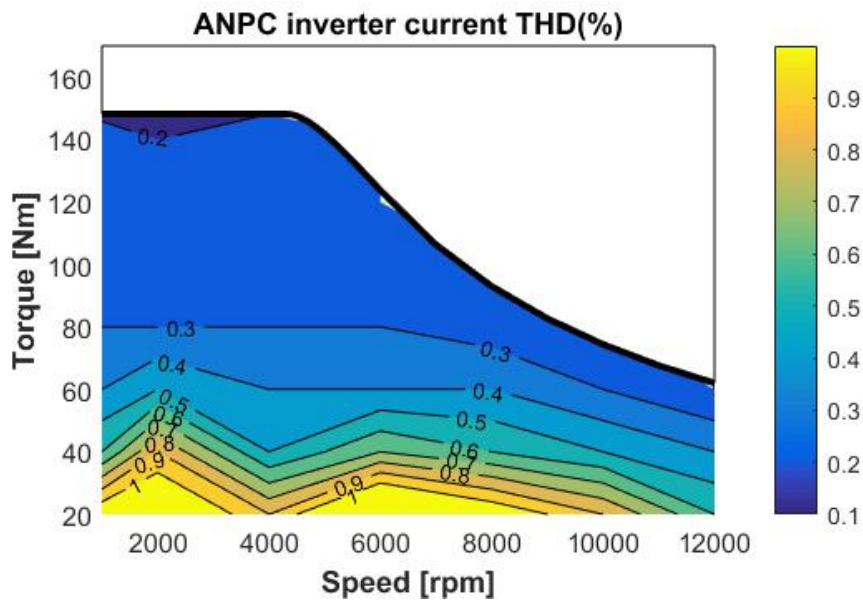


Figure 4.6: Current THD of the ANPC inverter

4.2.2 Losses and Efficiency Comparison

The power losses in inverters can be divided into two types of losses: conduction losses and switching losses. To conduct a more clear analysis of the losses in inverters, the two types of losses will be compared separately.

4.2.2.1 Conduction losses

Figure 4.7 and 4.8 show the conduction losses of the two-level inverter and the ANPC inverter. As is shown in the figures, the ANPC inverter produce more conduction losses in the whole area. This is because the ANPC inverter has more switches. As is shown in Figure 4.9, with the same output voltage and current, the current will pass through two switch devices in the ANPC inverter while only one switch device in the two-level inverter. Although the conduction losses of one switch device in the ANPC inverter is less than that in the two-level inverter, the number of conduction devices is twice. Thus the total conduction losses in the ANPC inverter is higher.

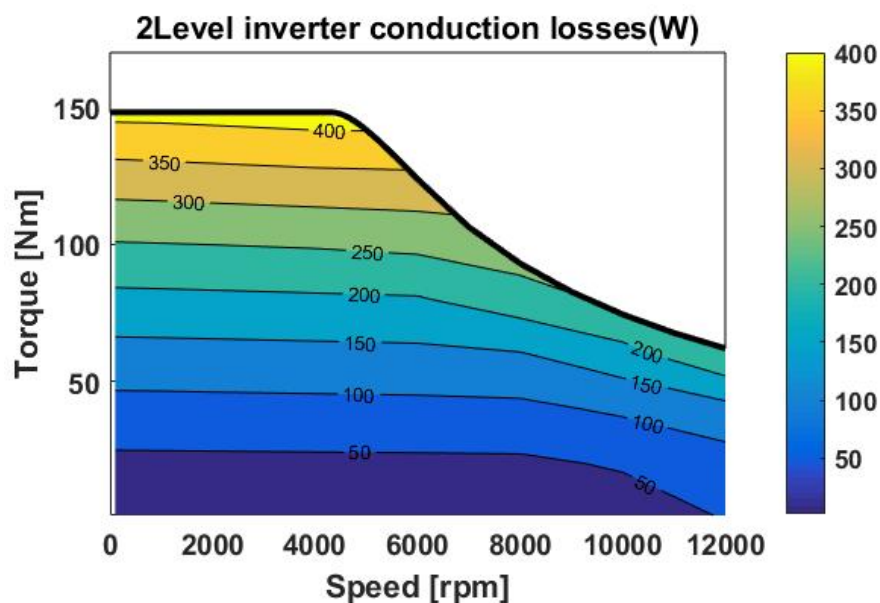


Figure 4.7: Conduction losses of the two-level inverter

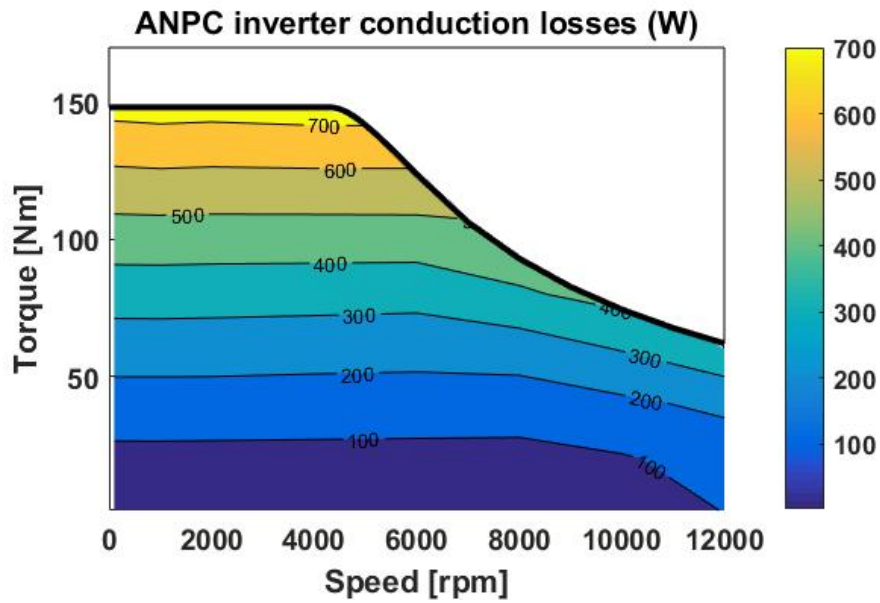


Figure 4.8: Conduction losses of the ANPC inverter

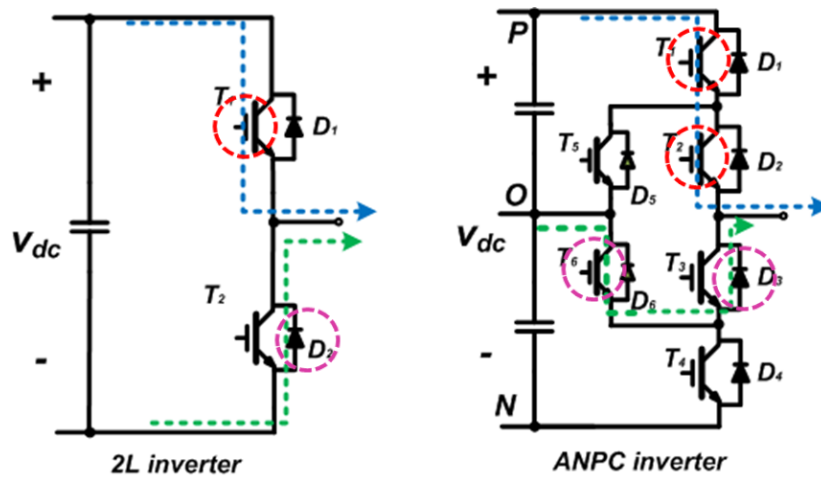


Figure 4.9: Current paths and conduction devices in inverters

4.2.2.2 Switching losses

The switching losses of the two-level inverter are shown in Figure 4.10 and of the ANPC inverter are shown in Figure 4.11. They show that the switching losses of the ANPC inverter is lower than that of the two-level inverter in the whole area. The reason is that the IGBT used in ANPC inverter has a much lower E_{on} and E_{off} , as is shown in Table 4.4. Moreover, as is shown in Figure 4.12, with the same output voltage and current, only two switches produce switching losses in both inverters.

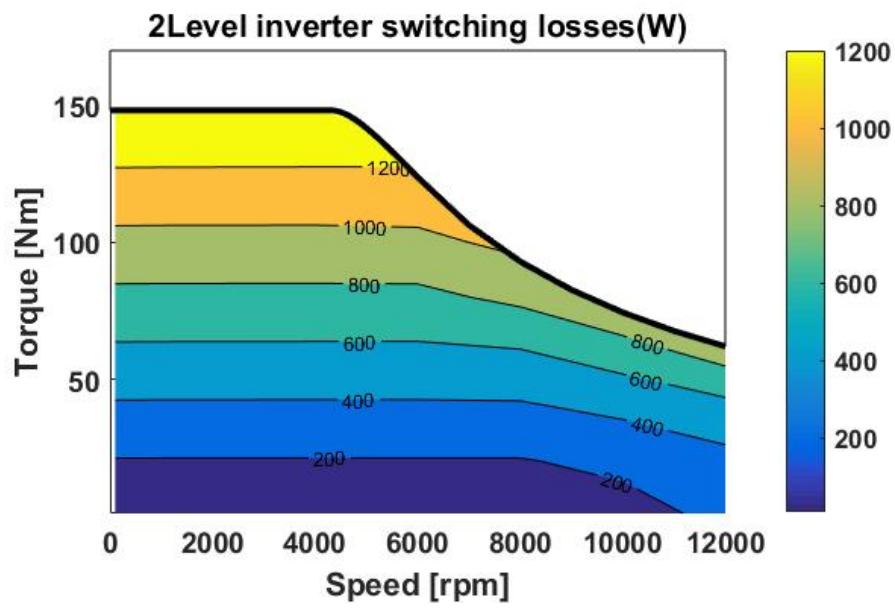


Figure 4.10: Switching losses of inverters

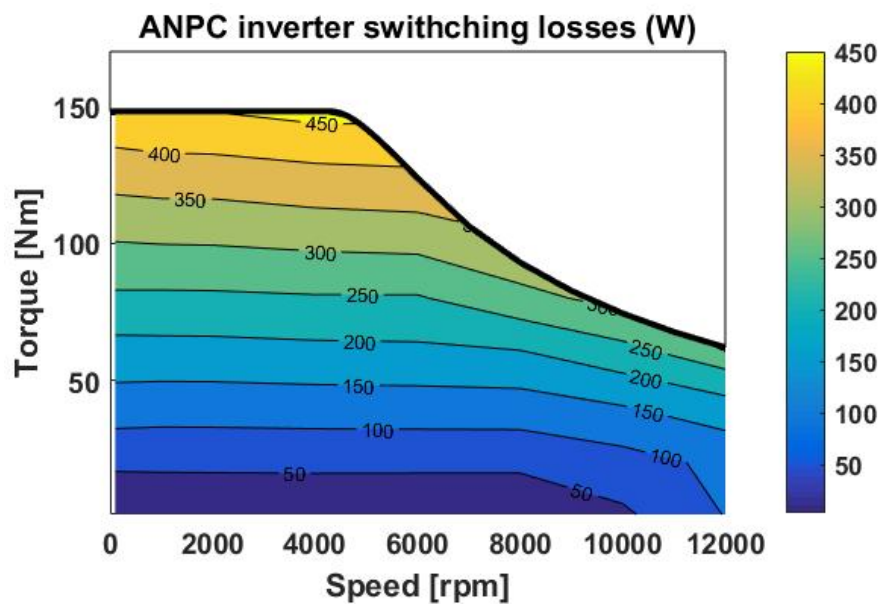


Figure 4.11: Switching losses of inverters

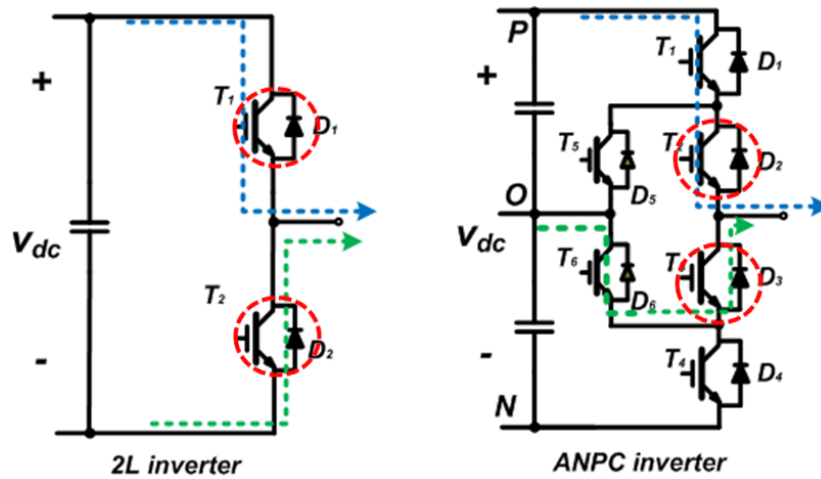


Figure 4.12: Current paths and switching devices in inverters

4.2.2.3 Total losses

The total power losses of the two inverters are shown in Figure 4.13 and Figure 4.14. To compare the total power losses of the two inverters more conveniently, Figure 4.15 shows the total power losses difference between the two inverters. As is shown in the figure, the ANPC inverter has lower power losses in the entire region.

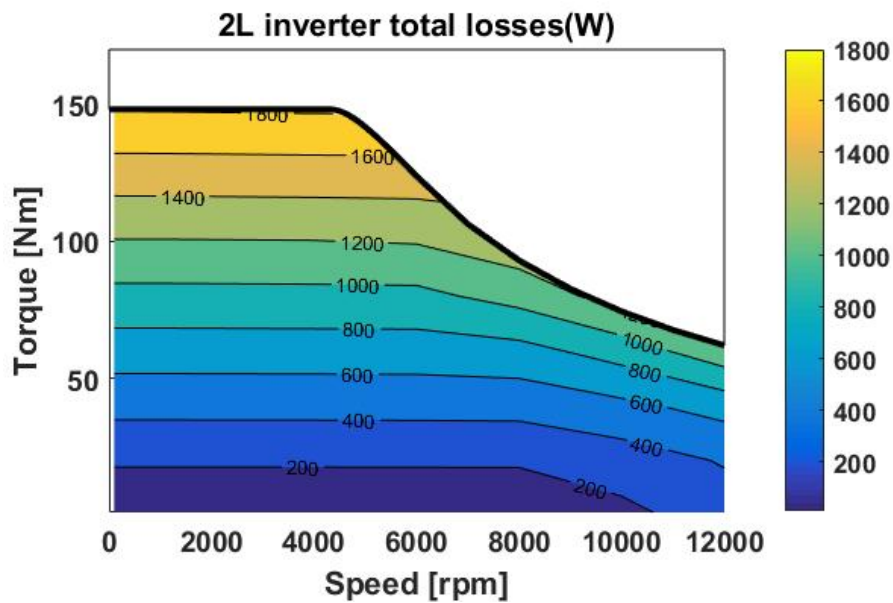


Figure 4.13: Total losses of inverters

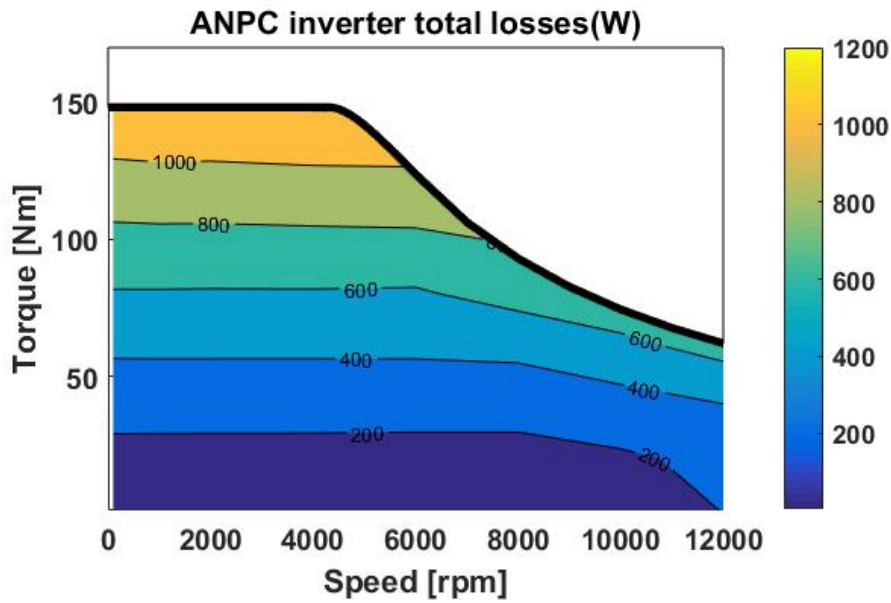


Figure 4.14: Total losses of inverters

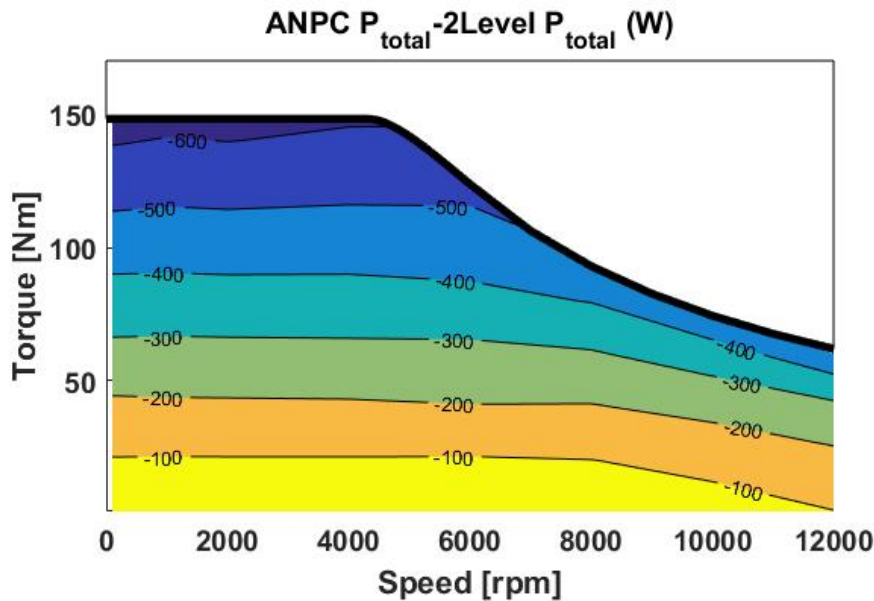


Figure 4.15: Total power losses difference of inverters

4.2.2.4 Efficiency

Figures 4.16 and 4.17 show the efficiency of the two-level inverter and the ANPC inverter. The efficiency of the ANPC inverter is higher than the two-level inverter in the entire region. However, in Figures 4.16 and 4.17, we should pay attention to the high speed low torque region. In this region, the field weakening method is used to make the electric machine operate at higher speed and the output active power is quite low, thus the output reactive power contributes to a large part of the total output power. However, the losses of the inverter are

related to the magnitude of the current including both active current and reactive current. Therefore, the efficiency in this region has an obvious reduction. Usually, the electric machine in electrified vehicles seldom operates in this area, thus the efficiency distortion in this area does not affect the efficiency performance of the inverter very much.

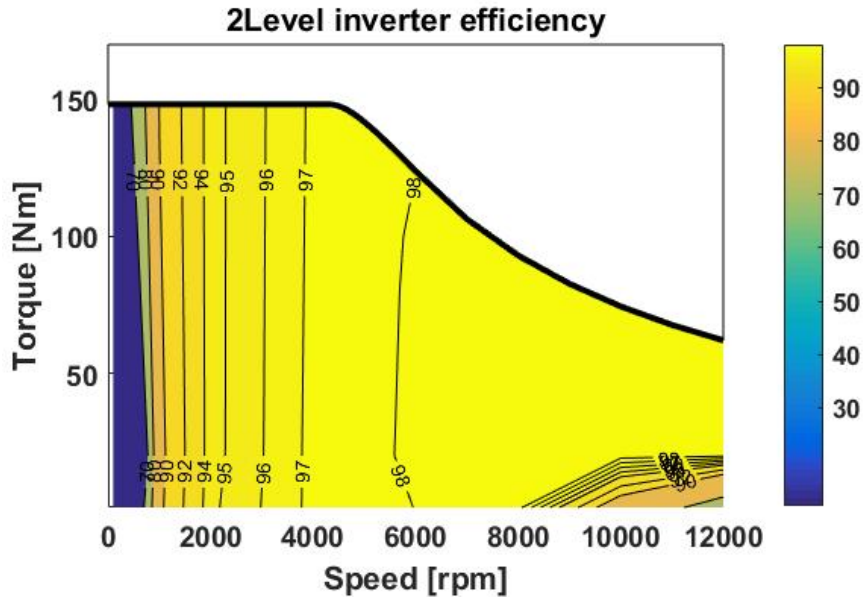


Figure 4.16: Efficiency of the two-level inverter

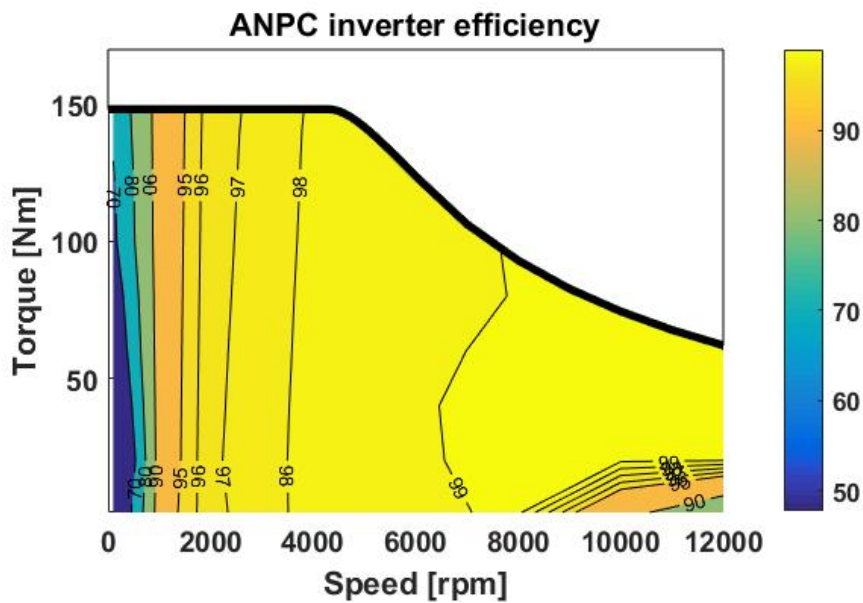


Figure 4.17: Efficiency of the ANPC inverter

4.2.3 Efficiency comparison with drive cycles

4.2.3.1 ECE drive cycle

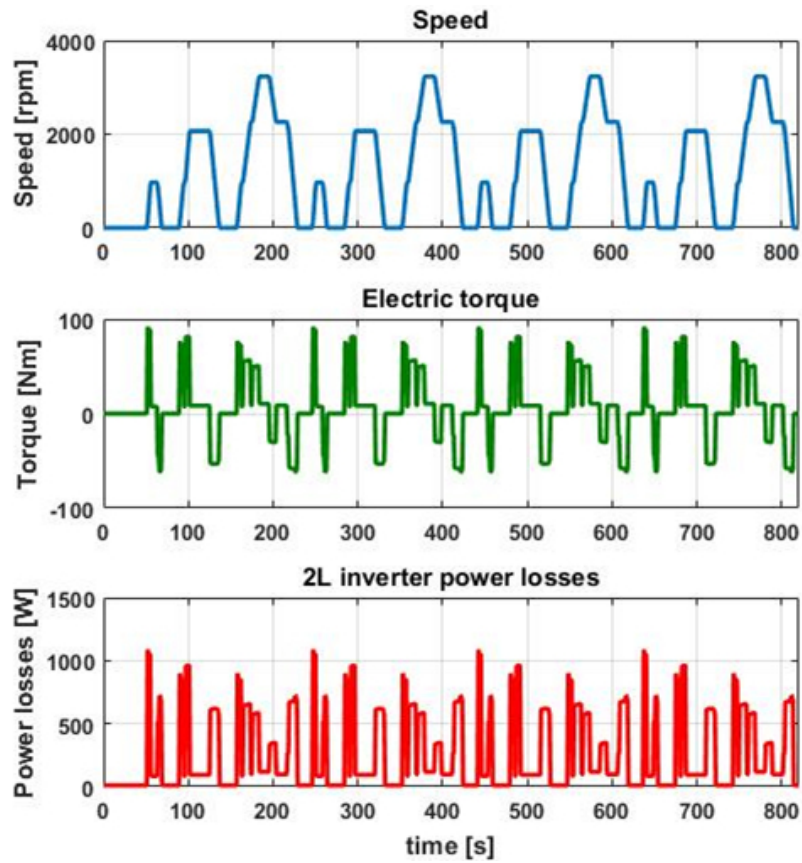


Figure 4.18: Power losses of the two-level inverter with the ECE drive cycle

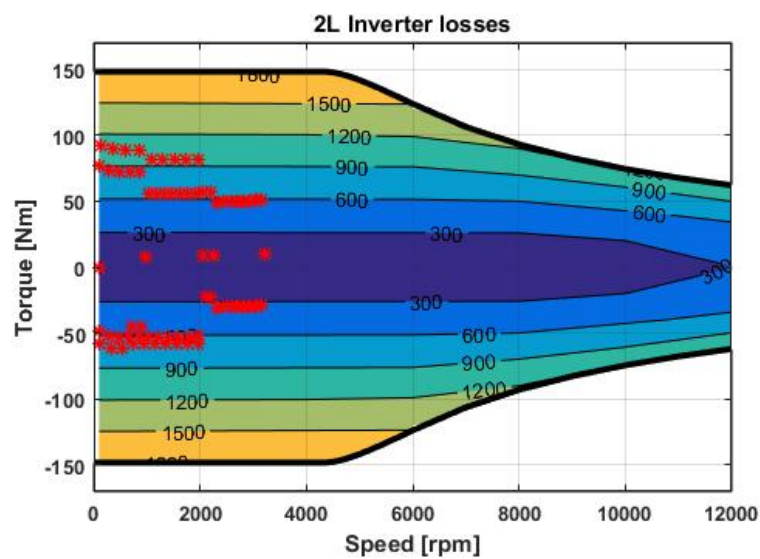


Figure 4.19: Power losses distribution of the two-level inverter with the ECE drive cycle

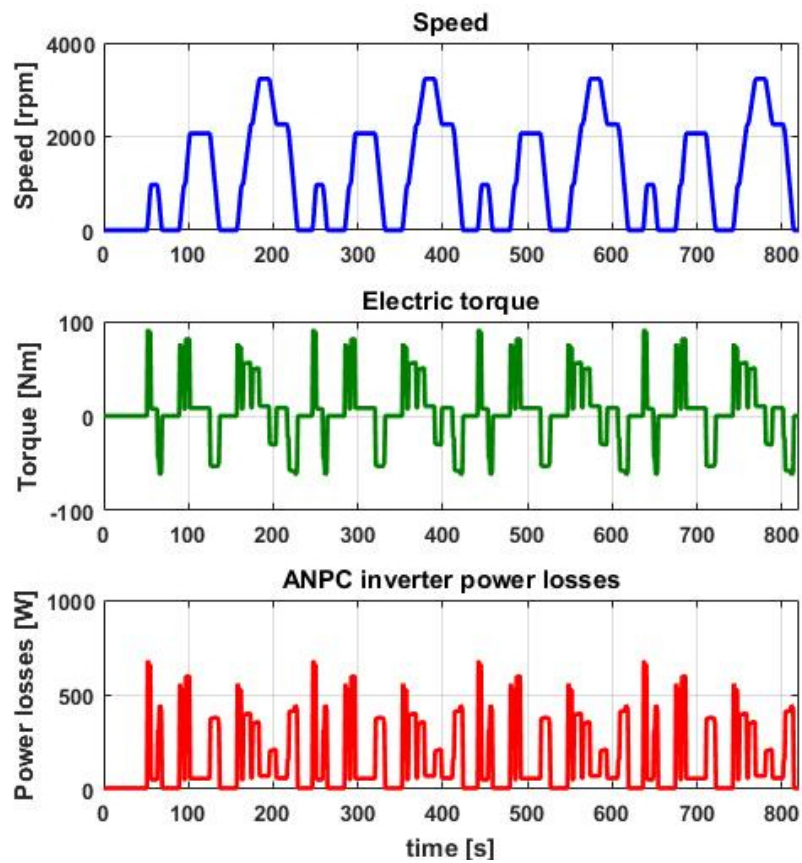


Figure 4.20: Power losses of the ANPC inverter with the ECE drive cycle

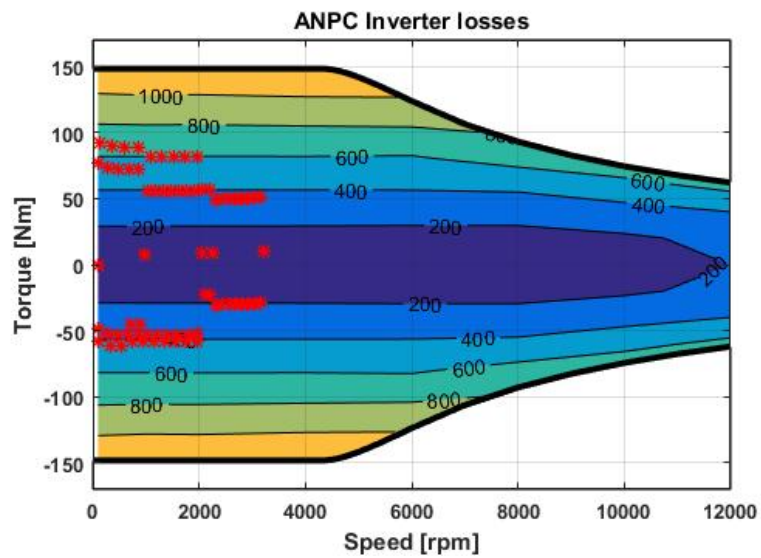


Figure 4.21: Power losses distribution of the ANPC inverter with the ECE drive cycle

4.2.3.2 EUDC drive cycle

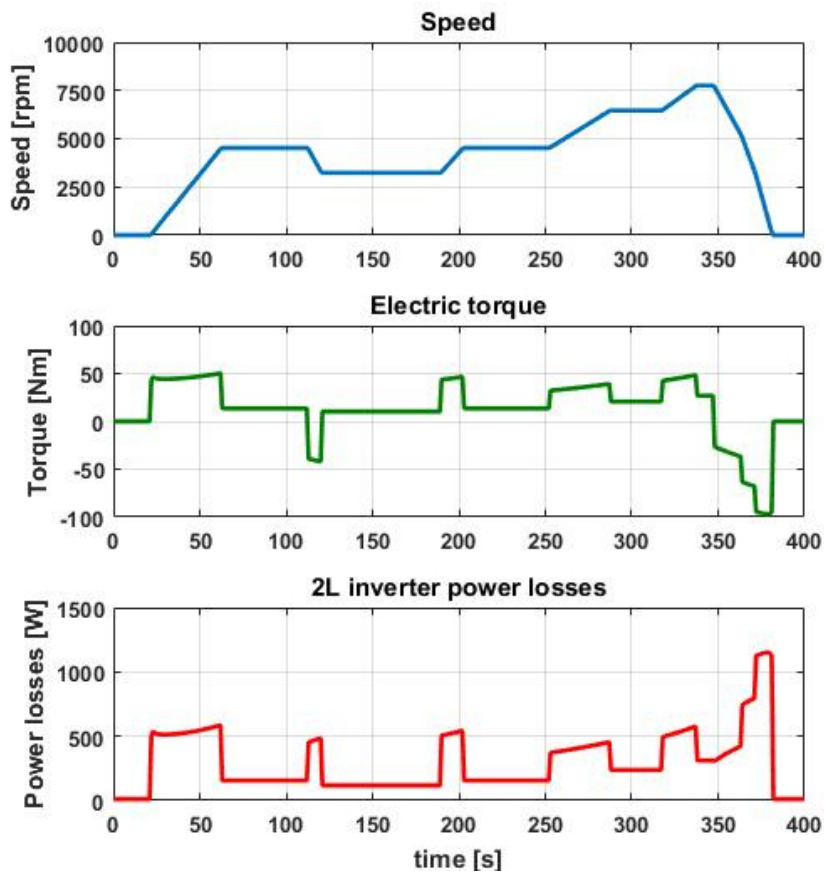


Figure 4.22: Power losses of the two-level inverter with the EUDC drive cycle

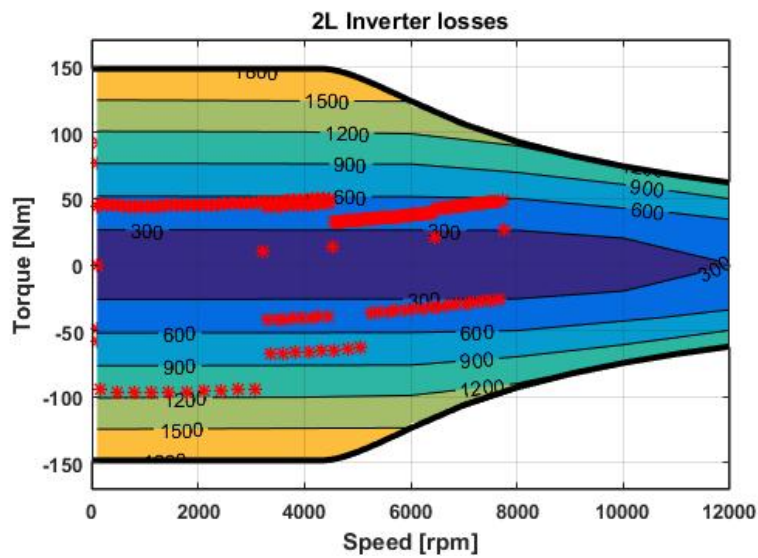


Figure 4.23: Power losses distribution of the two-level inverter with the EUDC drive cycle

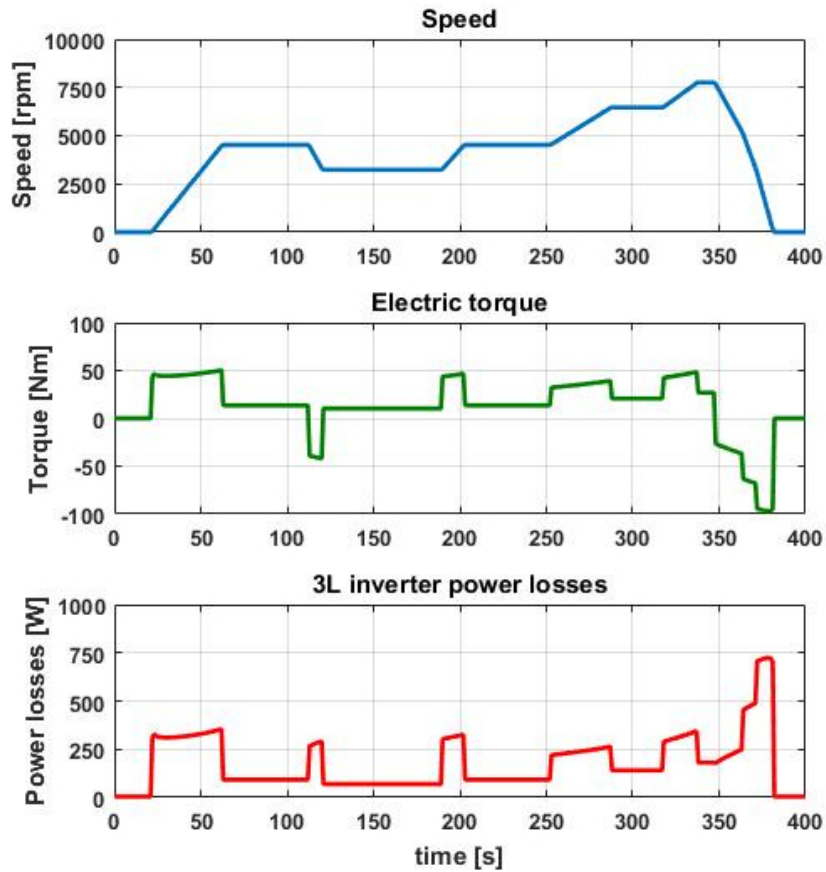


Figure 4.24: Power losses of the ANPC inverter with the EUDC drive cycle

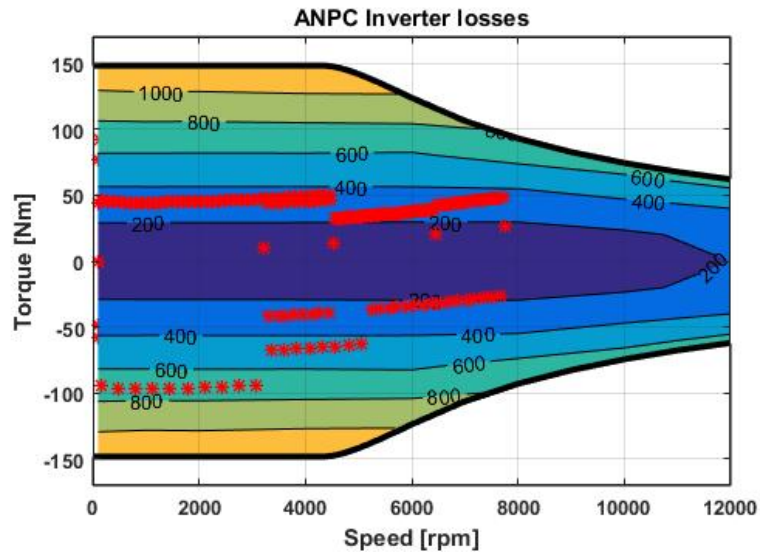


Figure 4.25: Power losses distribution of the ANPC inverter with the EUDC drive cycle

To evaluate the efficiency of the inverters in various drive cycles, the energy efficiency is more clear. The energy efficiency can be calculated as the total output energy divided by the sum of the total output energy and the total energy losses. The energy efficiency of the

Table 4.5: Drive cycle efficiency

Drive cycle	Efficiency (%)		
	Two-level inverter	ANPC inverter	Improvement
ECE	92.34	95.20	2.86
EUDC	97.49	98.48	0.99
NEDC	95.51	97.24	1.73

two-level inverter and the ANPC inverter in different drive cycles is shown in Table 4.5. The NEDC drive cycle is a combination of the ECE and EUDC drive cycles. As is shown in the table, the energy efficiency of the ANPC inverter has an improvement of 2.86% in the ECE drive cycle and 0.99% in the EUDC drive cycle.

4.3 Losses Distribution of the ANPC Inverter

The losses distributions of the ANPC inverter with different torques at speed 4000rpm are shown in Figure 4.26. As is shown in the figure, with increasing torque, the power losses for each device become larger. The distribution of the losses stay the same and the major losses always concentrate to the inner switch S_2 .

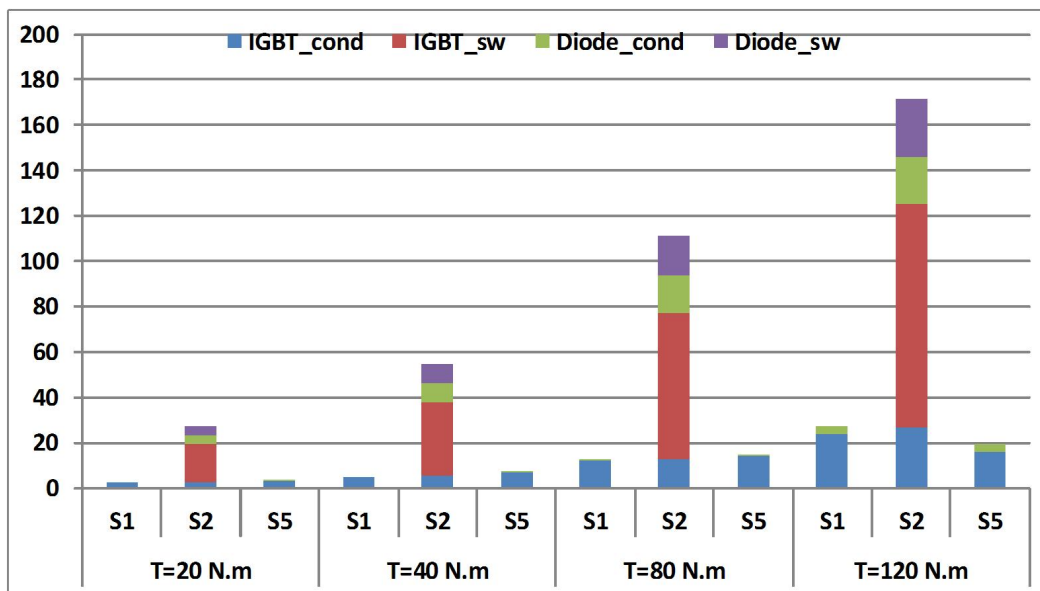


Figure 4.26: Losses distributions of the ANPC inverter at speed 4000 rpm

The losses distributions of the ANPC inverter with different speeds at torque 40N.m are shown in Figure 4.27. It shows that, with speed increasing, the total losses on the most stressed device S_2 varies slightly, the losses on S_5 reduced significantly while losses on S_1 have an obvious increment.

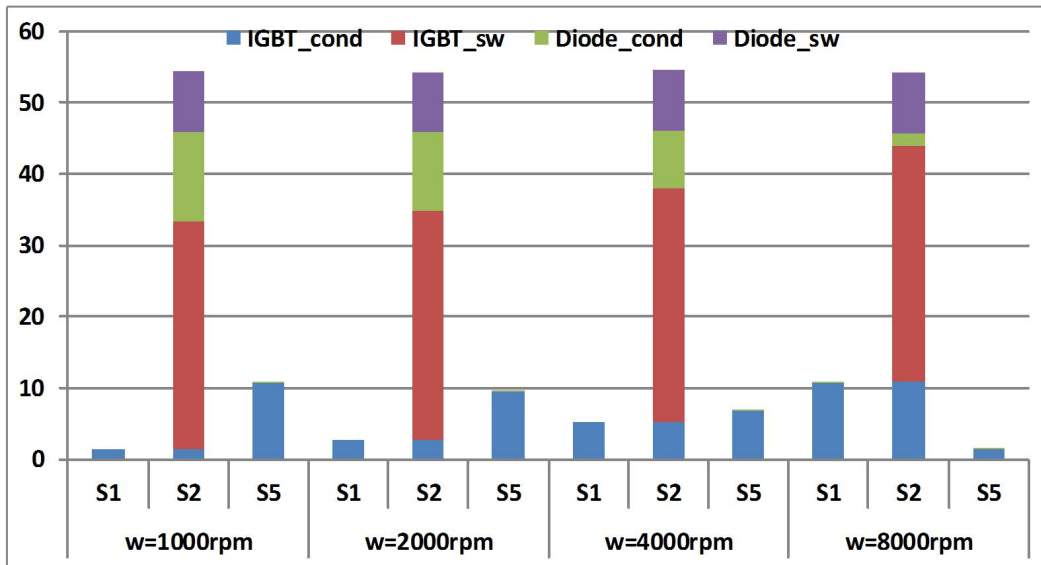


Figure 4.27: Losses distributions of the ANPC inverter at torque 40 N.m

The losses distribution of the ANPC inverter with various power factors is shown in Figure 4.28. It shows that the inner switch S_2 is the most stressed device regardless of the changing of power factor.

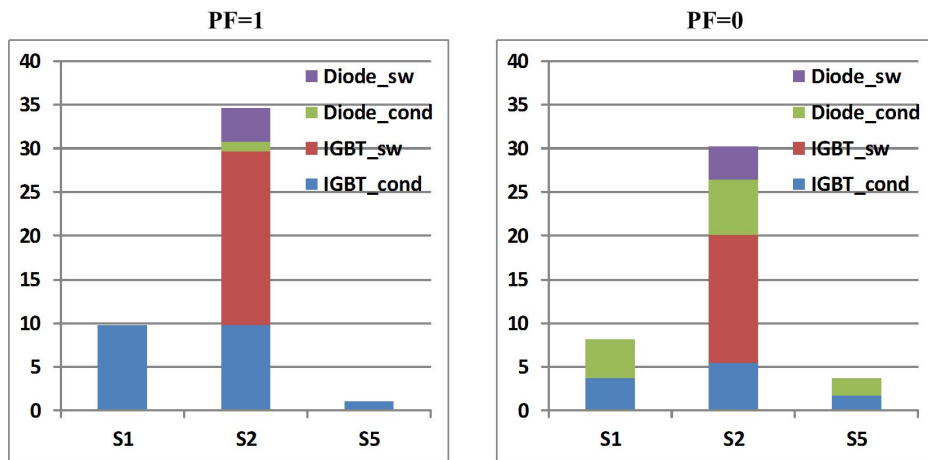


Figure 4.28: Losses distributions of the ANPC inverter with various power factors

5

Conclusion

In this thesis, an ANPC inverter for the PMSM motor drive in an electric vehicle has been implemented. The modulation strategy of the inverter is analyzed in detail and the SVM method is developed and carefully studied. Moreover, a two level inverter is implemented for performance comparison with the ANPC inverter. The comparison has been conducted in several aspects including power quality, total losses and efficiency as well as efficiency evaluation with various drive vehicles. Furthermore, the losses distribution in the ANPC inverter is also studied.

The development of the ANPC inverter has been carefully studied in the thesis. The modulation strategy of the ANPC inverter in the thesis is selected for minimizing switching actions and the SVM method is used for a higher utilization of the DC side voltage. A two-level inverter operate with SVM method is implemented for performance comparison.

The voltage stress for each switch in the ANPC inverter is much lower. With the 800V DC voltage, a switch with blocking voltage of 650V is selected in the ANPC inverter while the choice is a 1200V module in the two level inverter. Simulation results show that the output voltage and current of the ANPC inverter have better quality. The THD value has a maximum reduction of 101 % in voltage and 1.3 % in current respectively. Moreover, the ANPC converter has lower power losses in the entire operation region. It showed that the ANPC inverter can reach a maximum power efficiency of 99.25 % which is about 0.6 % higher than the two-level inverter. Furthermore, the average energy efficiency of the ANPC inverter improved 2.86 % when operating in the EUDC drive cycle and 0.99 % in the ECE drive cycle. The study of the losses distribution in the ANPC inverter shows that the losses distribute unevenly in the inverter but the most stressed device is the same regardless of changes of the voltage and current .

6

Future Work

Some possible work for continuation of this thesis are listed below.

First of all, the losses of the ANPC inverter can be reduced further by using several methods. As the current ripple of the ANPC inverter is lower than the two-level inverter, a lower switching frequency can be used in the ANPC inverter for the same current ripple. With reduced switching frequency, the losses will reduce subsequently. A new type SiC IGBT or a SiC MOSFET can be also be used in the ANPC inverter to achieve lower losses and higher efficiency.

Secondly, in the thesis the temperature influence on the power losses of the IGBT is ignored. While in the real case, the temperature is an important factor which will affect the losses. A more accurate losses calculation model includes the influence of temperature can be implemented to get close to the real application.

Thirdly, the losses distribute unevenly in the ANPC inverter with the modulation method used in the thesis. Different modulation methods can be used to make the losses distribution more even.

Moreover, for the multi-level inverter, the neutral point voltage balancing is usually an important issue. In the thesis, since the focus is on the power losses, the neutral point voltage control is ignored by using large capacitors at the DC side. However, in the real case, the capacitance of the DC side capacitor is limited thus the neutral point voltage control need to be considered.

References

- [1] Åström J. Investigation of Issues related to electrical efficiency improvements of pump and fan drives in buildings[J]. 2008.
- [2] Cavallaro C, Tommaso A O D, Miceli R, et al. Efficiency enhancement of permanent-magnet synchronous motor drives by online loss minimization approaches[J]. *Industrial Electronics, IEEE Transactions on*, 2005, 52(4): 1153-1160.
- [3] Vollmer U, Schäfer U. An At-All Operating Points Highly Efficient PMSM for HEV[J]. *The World Electric Vehicle Journal*, 2008, 2(4).
- [4] Cvetkovski G, Petkovska L. Efficiency maximisation in structural design optimisation of permanent magnet synchronous motor[C]//*Electrical Machines*, 2008. ICEM 2008. 18th International Conference on. IEEE, 2008: 1-6.
- [5] Hassan W, Wang B. Efficiency optimization of PMSM based drive system[C]//*Power Electronics and Motion Control Conference (IPEMC)*, 2012 7th International. IEEE, 2012, 2: 1027-1033.
- [6] Tolbert L M, Ozpineci B, Islam S K, et al. Impact of SiC power electronic devices for hybrid electric vehicles[C]//*2002 Future Car Congress Proceedings*. 2002: 3-5.
- [7] Ozpineci B, Tolbert L M, Islam S K. Silicon carbide power device characterization for HEVs[C]//*Power Electronics in Transportation*, 2002. IEEE, 2002: 93-97.
- [8] Ozpineci B, Tolbert L M, Islam S K, et al. Effects of silicon carbide (SiC) power devices on HEV PWM inverter losses[C]//*Industrial Electronics Society*, 2001. IECON'01. The 27th Annual Conference of the IEEE. IEEE, 2001, 2: 1061-1066.
- [9] Teichmann R, Bernet S. A comparison of three-level converters versus two-level converters for low-voltage drives, traction, and utility applications[J]. *IEEE Transactions on Industry Applications*, 2005, 41(3): 855-865.
- [10] Chen Z, Yuan L, Zhao Z, et al. Power losses in two-and three-level three phase photovoltaic inverters equipped with IGBTs[C]//*Electrical Machines and Systems (ICEMS)*, 2012 15th International Conference on. IEEE, 2012: 1-6.
- [11] L. M. Tolbert, F. Z. Peng, T. Cunnyngham, and J. N. Chiasson, "Chargebalance control schemes for cascaded multilevel converter in hybrid electricvehicles," *IEEE Trans. Ind. Electron.*, vol. 49, no. 5, pp. 1058–1064, Oct.2002
- [12] L. M. Tolbert, F. Z. Peng, and T. G. Habetler, "Multilevel converters forlarge electric

- drives,” *IEEE Trans. Ind. Appl.*, vol. 35, no. 1, pp. 36–44, Jan./Feb. 1999.
- [13] Choudhury A, Pillay P, Williamson S S. DC-link voltage balancing for a three-level electric vehicle traction inverter using an innovative switching sequence control scheme[J]. *Emerging and Selected Topics in Power Electronics, IEEE Journal of*, 2014, 2(2): 296-307.
- [14] Rodriguez. Jose, Bernet. Steffen, Steimer. Peter, K. Lizama, Ignacio E, A Survey on Neutral-Point-Clamped Inverters, *IEEE Trans on Industry Electrics*, 57(1), 2219-2230., 2010.
- [15] Andler, D., et al.. Experimental Investigation of the Commutations of a 3L-ANPC Phase Leg Using 4.5-kV - 5.5-kA IGCTs. *IEEE Transactions on Industrial Electronics*, 60(11): 4820-4830, 2013.
- [16] T. Brückner, S. Bernet, H. Güldner, “The Active NPC Converter and Its Loss-Balancing Control,” *IEEE Transactions on Industrial Electronics*, Vol. 52, No. 3, pp. 855–868, June 2005. AS
- [17] Jing X, He J, Demerdash NAO. Application and losses analysis of ANPC converters in doubly-fed induction generator wind energy conversion system[C]. *Electric Machines and Drives Conference (IEMDC), 2013 IEEE International. IEEE*, 2013: 131-138.
- [18] Sankar A B, Seyezhai R. Development of active neutral point clamped multilevel inverter fed BLDC drive employing FPGA[J]. *Indian Journal of Science and Technology*, 2015, 8(4): 392-399.
- [19] Bolognani S, Morandini M, Calligaro S, et al. Bidirectional PMSM drive employing a three level ANPC inverter and a multi-phase interleaved DC/DC converter for hybrid electric vehicles[C]. *Applied Power Electronics Conference and Exposition (APEC), 2014 Twenty-Ninth Annual IEEE. IEEE*, 2014: 818-825.
- [20] Datasheet FF450R07ME4-B11, Infineon, 2014-12-15, Rev.3.1.
- [21] Datasheet FF450R12ME4-B11, Infineon, 2013-11-05, Rev.2.0.